Quaternary Geochronology 39 (2017) 1–23

Contents lists available at ScienceDirect

Quaternary Geochronology

journal homepage: www.elsevier.com/locate/quageo

Research paper

High-precision $^{40}Ar/^{39}Ar$ dating of pleistocene tuffs and temporal anchoring of the Matuyama-Brunhes boundary

Darren F. Mark [a, b, *], Paul R. Renne [c, d], Ross C. Dymock [a], Victoria C. Smith [e], Justin I. Simon [f], Leah E. Morgan [a, g], Richard A. Staff [e], Ben S. Ellis [g], Nicholas J.G. Pearce [h]

[a] Scottish Universities Environmental Research Centre, Isotope Geosciences Unit, Rankine Avenue, East Kilbride, Scotland, G75 0QF, UK
[b] Department of Earth & Environmental Science, School of Geography & Geosciences, University of St Andrews, St Andrews, KY16 9AJ, UK
[c] Berkeley Geochronology Center, 2455 Ridge Rd., Berkeley, CA, 94709, USA
[d] Department of Earth and Planetary Science, University of California, Berkeley, CA, 94720, USA
[e] Research Laboratory for Archaeology and the History of Art, University of Oxford, Oxford, OX1 3QY, UK
[f] Center for Isotope Cosmochemistry and Geochronology, Astromaterials Research Office KR111, NASA Johnson Space Center, Houston, TX, 77058, USA
[g] Institute of Geochemistry and Petrology, Department of Earth Sciences, ETH Zurich, Clausiusstrasse 25, 8092, Zürich, Switzerland
[h] Department of Geography and Earth Sciences, Aberystwyth University, Aberystwyth, SY23 3DB, UK

ARTICLE INFO

Article history:
Received 6 February 2016
Received in revised form
10 January 2017
Accepted 15 January 2017
Available online 18 January 2017

Keywords:
Matuyama-Brunhes
Geomagnetic
$^{40}Ar/^{39}Ar$
Toba
Bishop tuff
Orbital tuning
Australasian tektite

ABSTRACT

High-precision $^{40}Ar/^{39}Ar$ ages for a series of proximal tuffs from the Toba super-volcano in Indonesia, and the Bishop Tuff and Lava Creek Tuff B in North America have been obtained. Core from Ocean Drilling Project Site 758 in the eastern equatorial Indian Ocean contains discrete tephra layers that we have geochemically correlated to the Young Toba Tuff (73.7 ± 0.3 ka), Middle Toba Tuff (502 ± 0.7 ka) and two eruptions (OTTA and OTTB) related to the Old Toba Tuff (792.4 ± 0.5 and 785.6 ± 0.7 ka, respectively) ($^{40}Ar/^{39}Ar$ data reported as full external precision, 1 sigma). Within ODP 758 Termination IX is coincident with OTTB and hence this age tightly constrains the transition from Marine Isotope Stage 19–20 for the Indian Ocean. The core also preserves the location of the Australasian tektites, and the Matuyama-Brunhes boundary with Bayesian age-depth models used to determine the ages of these events, c. 786 and c. 784 ka, respectively. In North America, the Bishop Tuff (766.6 ± 0.4 ka) and Lava Creek Tuff B (627.0 ± 1.5 ka) have quantifiable stratigraphic relationships to the Matuyama-Brunhes boundary. Linear age-depth extrapolation, allowing for uncertainties associated with potential hiatuses in five different terrestrial sections, defines a geomagnetic reversal age of 789 ± 6 ka. Considering our data with respect to the previously published age data for the Matuyama-Brunhes boundary of Sagnotti et al. (2014), we suggest at the level of temporal resolution currently attainable using radioisotopic dating the last reversal of Earths geomagnetic field was isochronous. An overall Matuyama-Brunhes reversal age of 783.4 ± 0.6 ka is calculated, which allowing for inherent uncertainties in the astronomical dating approach, is indistinguishable from the LR04 stack age (780 ± 5 ka) for the geomagnetic boundary. Our high-precision age is 10 ± 2 ka older than the Matuyama-Brunhes boundary age of 773 ± 1 ka, as reported previously by Channell et al. (2010) for Atlantic Ocean records. As ODP 758 features in the LR04 marine stack, the high-precision $^{40}Ar/^{39}Ar$ ages determined here, as well as the Matuyama-Brunhes boundary age, can be used as temporally accurate and precise anchors for the Pleistocene time scale.

1. Introduction

The Earth's magnetic field alternates between periods of *normal* polarity, in which the mean polarity of the field was the same as the present, and *reverse* polarity, in which the polarity was the opposite. Reversals in geomagnetic field polarity have occurred episodically throughout much of geologic time. To the extent that these polarity reversals are globally synchronous they can be used as tick marks whose ages, when calibrated, are invaluable components of the Geological Time Scale. Two challenges limit the utility of geomagnetic polarity reversals as time stamps in the geologic

* Corresponding author. Scottish Universities Environmental Research Centre, Isotope Geosciences Unit, Rankine Avenue, East Kilbride, Scotland, G75 0QF, UK.
E-mail address: darren.mark@glasgow.ac.uk (D.F. Mark).

http://dx.doi.org/10.1016/j.quageo.2017.01.002

record: (1) the unambiguous correlation of magnetic polarity records recovered from rocks or sediments with a global record of such events, and (2) the accuracy of age calibrations. In this paper we address both issues in the case of the reversal between the Matuyama and Brunhes geomagnetic polarity epochs, also known as the Matuyama-Brunhes boundary (MBB), whose age is of fundamental importance to many topics in the Earth Sciences yet has been controversial.

The MBB was the most recent full reversal of the Earth's magnetic field, and serves as a Global Boundary Stratotype Section and Point (GSSP), selected by the International Commission on Stratigraphy as a marker for the beginning of the Middle Pleistocene. An age of 780 ka for the MBB (Shackleton et al., 1990) was determined by orbital tuning of benthic and planktic $\partial^{18}O$ records from Ocean Drilling Program (ODP) Site 677 in the eastern equatorial Pacific (Fig. 1). The tuning was calibrated to an ice volume model (Imbrie and Imbrie, 1980), which was based on a series of orbital solutions (Berger and Loutre, 1988). The specific location of the MBB within the ODP 677 core was unknown and hence extrapolation of its location from Deep Sea Drilling Project Site 607 was required (Fig. 1). Other orbital tuning ages for the MBB range from 730 ka (Imbrie et al., 1984; Ruddiman et al., 1989) to 790 ka (Johnson, 1982).

An extremely precise orbitally-tuned age of 773 ± 1 ka was recently proposed for the MBB (Channell et al., 2010). Five North Atlantic records placed in isotope age models that were constructed by correlation of the $\partial^{18}O$ record directly or indirectly to an ice volume model were used to place the MBB consistently at the young end of Marine Isotope Stage (MIS) 19. The orbitally-tuned MBB age inferred by Channell et al. (2010) was stated to be consistent with an $^{40}Ar/^{39}Ar$ age (776 ± 2 ka, 1 sigma, analytical uncertainty only) (Coe et al., 2004), from Hawaiian lavas, but only if the age of Fish Canyon sanidine (FCs), a secondary mineral standard

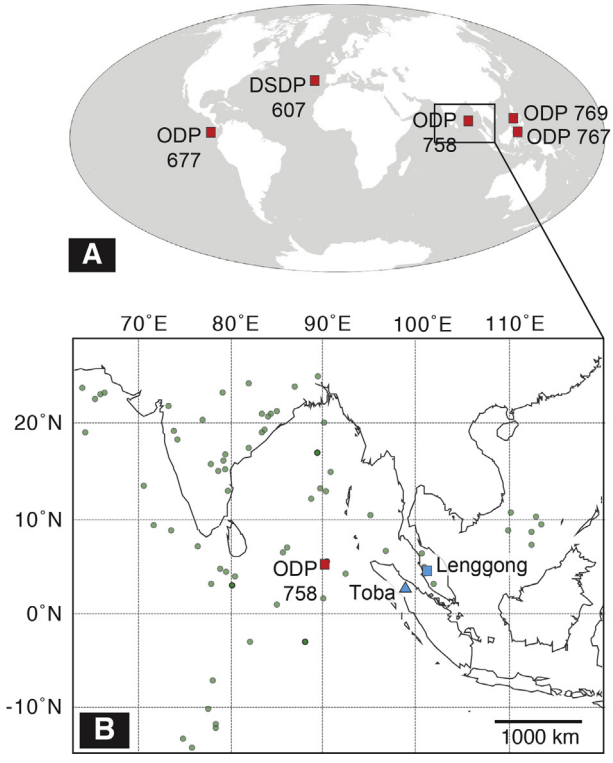

Fig. 1. (A) World map showing the locations of marine cores referred to in main text. (B) Map showing location of ODP 758 relative to Sumatra and Toba as well as the known distribution of Toba eruptive deposits throughout the region (green dots). (For interpretation of the references to colour in this figure legend, the reader is referred to the web version of this article.)

for the $^{40}Ar/^{39}Ar$ radio-isotopic dating system, is adjusted to an age of 27.93 Ma – an age known from numerous studies to be too young (e.g., Kuiper et al., 2008; Renne et al., 2011; Rivera et al., 2011; Wotzlaw et al., 2013; Morgan et al., 2014). Remarkably, Singer (2014) subsequently reanalysed the same Hawaiian lavas and obtained the identical result of 776 ± 1 ka (1 sigma, analytical uncertainty only) but using a different $^{40}Ar/^{39}Ar$ calibration (decay constants of Min et al., 2000; the FCs age of 28.201 Ma, Kuiper et al., 2008). The perfect congruence of these two ages is spurious, however, as applying the same calibration to both $^{40}Ar/^{39}Ar$ ages (Coe et al., 2004; Singer, 2014) indicates that they differ by 5 ± 3 ka.

Direct radio-isotopic ages have been determined for the MBB through $^{40}Ar/^{39}Ar$ dating of various lava flows with transitional directions or known relationships to the MBB. Baksi et al. (1992) dated lavas from Maui with transitional paleomagnetic directions related to the MBB to yield an $^{40}Ar/^{39}Ar$ age of 783 ± 11 ka (1 sigma, analytical uncertainty only) using the decay constants of Steiger and Jager (1977) and the SB3 biotite standard at 162.9 Ma, which is equivalent to Fish Canyon sanidine (FCs) at 27.5 Ma (Lanphere and Baadsgaard, 2001). Recalculated[1] this age is 795 ± 11/12 ka. Singer and Pringle (1996) determined an $^{40}Ar/^{39}Ar$ weighted mean age for 8 basaltic to andesitic lava flows inferred to have erupted during the MB-reversal from Chile, Tahiti, La Palma and Maui. They calculated an age (779 ± 2 ka, 1 sigma, analytical) using the decay constants of Steiger and Jager (1977) and the Taylor Creek sanidine (TCs) standard with an age of 27.9 Ma, which is also equivalent to FCs at 27.5 Ma. Recalculated the MBB age of Singer and Pringle (1996) is 791 ± 2/3 ka. Singer et al. (2005) incorporating the data of Coe et al. (2004) proposed that there were two age clusters for MBB-related lava flows: (1) 776 ± 2 ka (1 sigma, analytical uncertainty), and (2) 793 ± 3 ka (1 sigma, analytical uncertainty). These ages were calculated using the decay constants of Steiger and Jager (1977) and TCs with an age of 28.34 Ma, which is equivalent to an FCs age of 28.02 Ma (Renne et al., 1998). Recalculated these ages are 773 ± 2/3 ka and 790 ± 3/3 ka, respectively. It was proposed that the older age was related to an initial demise of the axial dipole, onset of geodynamo instability, and non-dipolar field behaviour – a precursor to reversal of field polarity. A MBB precursor event with low field intensity has been noted in some (Kent and Schneider, 1995; Hartl and Tauxe, 1996; Channell et al., 2009, 2010) but not all marine records (e.g., Suganuma et al., 2015). Importantly, there is no direct palaeomagnetic evidence linking the older age of Singer et al. (2005) to such a precursor event. As discussed (above), Singer (2014) made new measurements on old MBB-related samples (Coe et al., 2004), giving a recalculated age of 779 ± 1/1 ka.

The dating of silicic tuffs that straddle the MBB has vast potential for determination of accurate and precise event timings with robust, fully quantifiable uncertainties, especially if high-K phases such as sanidine/anorthoclase are present for $^{40}Ar/^{39}Ar$ analyses. The sanidine- and zircon-bearing Bishop Tuff (BT) deposited below the Lava Creek Tuff Member B (LCTB) but above the MBB, has been the focus of much interest. Briefly, Sarna-Wojcicki et al. (2000) calculated sedimentation rates in terrestrial sections throughout western North America making the simple (but geologically tenuous) assumption of constant sedimentation rate between the LCTB and the BT. Employing the inferred sedimentation rates, they calculated the duration between the BT and the MBB represented

[1] Unless otherwise stated all $^{40}Ar/^{39}Ar$ ages are re-calculated using the optimisation model of Renne et al. (2010), the decay constants of (Renne et al., 2011) and an Alder Creek sanidine (ACs) age of 1.1891 Ma (Niespolo et al., 2016). All data are reported as X ± Y/Z, where Y is analytical uncertainties and Z is full external precision, including uncertainties from the decay constant. The confidence interval is 68.2% confidence (1 sigma).

by the intervening sediment. These results, that are independent of which calibration of the $^{40}Ar/^{39}Ar$ system is used, imply that the MBB is 15 ± 2 ka older than the BT if the assumption of uniform sedimentation is correct. Unfortunately, the age of the Bishop Tuff has remained controversial and hence its reliability for determination of an age for the MBB has been questioned (e.g., Channell et al., 2010).

The age, character and tempo of the MBB was clarified by recent high-precision $^{40}Ar/^{39}Ar$ dating of sanidine from tephra layers that bracket the boundary within the Sulmona Basin paleolake in Central Italy (Sagnotti et al., 2014; Giaccio et al., 2015). The lacustrine sediments within which the tuffs are intercalated are characterized by biogenic magnetite and were sampled at high resolution, allowing the reconstruction of the MBB in very fine detail. The Sulmona results show that the MBB is significantly older than 773 ± 1 ka (Channell et al., 2010) with a recalculated age of 783 ± 1/1 ka. Using the same parameters but the weighted mean astronomical ACs age rather than the Optimisation Model ACs age (Niespolo et al., 2016), the Sulmona data yield a MBB age of 780 ± 1/1 ka (Sagnotti et al., 2014), both ages resolvably older (10 ± 2 ka and 7 ± 2 ka, respectively) than 773 ± 1 ka.

Most recently U-Pb SHRIMP-II ages have been determined for a tephra associated with the MBB in Japan (Suganuma et al., 2015). However, primarily for reasons highlighted by Ickert et al. (2015) and discussed by us in detail below, we do not consider either the U/Pb data accurate or appropriate for use in determining an age for the MBB (i.e., poor characterisation of Th/U_{melt} from which the zircons grew). Further, Suganuma et al. (2015) failed to disequilibrium-correct their Tera-Wasserburg relations, the oxygen isotope data are of inadequately low resolution to precisely define the boundaries of MIS 19, and there are no quantitative constraints for the sedimentation rate.

1.1. The MB-reversal: isochronous or diachronous?

Owing to large degrees of scatter in the data that attempt to temporally anchor the MBB there has been the suggestion that the reversal was diachronous on a global-scale (e.g., Rivera et al., 2011). Until recently the MB-reversal, as with other geomagnetic polarity reversals, has been considered isochronous, certainly at the relatively poor levels of temporal resolution (accuracy and precision) attained using the $^{40}Ar/^{39}Ar$ geochronometer between 1990 and 2010. However, computer modeling of the MB-reversal has highlighted potential for a millennial-scale (±1 ka) offset in the onset of the polarity reversal for sites in the Atlantic and Pacific Oceans (Leonhardt and Fabian, 2007). The study also proposed reversal durations of between 2 and 10 ka, which exceeds the MBB duration recorded by the high-resolution record at Sulmona by more than an order of magnitude (Sagnotti et al., 2016).

1.2. Ocean Drilling Project (ODP) Leg 758

Ocean Drilling Project (ODP) Site 758 resides on the crest of Ninetyeast Ridge (5°23.05′N, 90°21.67′E) in a water depth of 2924 m (Fig. 1). Three holes were cored at Site 758 (A, B, C). Within the timeframe of interest (Holocene-Pleistocene) stratigraphic analysis showed good recovery (Shipboard Scientific Party, 1989). Due to the possibility of gaps occurring between successive Advanced Piston Corer (APC) core sections, sections in ODP 758A and ODP 758B were staggered in depth relative to each other. It was possible to provide high-resolution between-hole correlation by using a combination of paleomagnetic remanence, magnetic susceptibility and distinct lithological and tephra markers (Shipboard Scientific Party, 1989; Dehn et al., 1991; Farrell and Janecek, 1991; Gee et al., 1991).

There were two defined scientific aims for drilling Site 758: (1) to study the tephrochronology of the Indonesian volcanic arc relative to a changing climate signal, and (2) to study in detail the behaviour of Earth's magnetic field during polarity transitions. As such the ODP 758 deep sea core contains: (1) records of distal tephras (volcanic ash layers) from the Indonesian volcanic arc above and below the MBB (Dehn et al., 1991), (2) cm-scale resolution $\partial^{18}O$ records from benthic and planktic foraminifera (Farrell and Janecek, 1991; Chen et al., 1995), and (3) a detailed paleomagnetic stratigraphy that shows the precise and well-defined location of the MBB, as well as the onset and termination of the Jaramillo Geomagnetic Excursion (JGE) (Shipboard Scientific Party, 1989; Gee et al., 1991).

1.3. ODP 758 tephrochronology

The tephra layers documented within Site 758 provide a unique record of explosive volcanism for the North Indian Ocean. Over 200 visible tephra (ash) layers have been documented from the site ranging in thickness from millimetres to decimetres. Many of the tephras are present in one hole but not in the neighbouring holes. The tephras also display variable forms, ranging from discrete to diffuse layers and patches/pods of ash. The local absence and variable physical characteristics of a given tephra is due to the variety of depositional processes operating on the crest of the Ninetyeast Ridge (Dehn et al., 1991) and hence not unexpected (Carey, 1997). Given the distance (Fig. 1) between Site 758 and the Indonesian volcanic arc (the most proximal and therefore probable volcanic source) the tephra found in the three holes are distal in nature, fine-grained and dominated by glass shards rather than mineral grains. As such the tephras are unsuitable for direct $^{40}Ar/^{39}Ar$ dating due to paucity of required mineral phases.

Two of the distal tephras located in ODP 758 have been robustly correlated using glass and mineral chemistry to the Young Toba Tuff (YTT, Ash A, *c.* 74 ka; Mark et al., 2014; Storey et al., 2012) and Middle Toba Tuff (MTT, Ash C, *c.* 500 ka; Chesner et al., 1991) eruptions of the Toba super-volcano (Dehn et al., 1991) (Fig. 1). Older ash units (E, *d* and D) have been the focus of much attention with the question raised as to which, if any, correlates with the oldest super-eruption (Old Toba Tuff, OTT, *c.* 800 ka; Chesner et al., 1991) of Toba (Shane et al., 1995). Lee et al. (2004) linked Ash D with OTT but this correlation was subsequently questioned (Chen et al., 2004; Shane et al., 2004). Further geochemical work is required to confidently link these ashes to proximal deposits, and to determine whether or not their source was indeed Toba. Note, the age of Ash D was calibrated by astronomically tuned oxygen isotope stratigraphy to 788.0 ± 2.2 ka (Lee et al., 2004).

1.4. Paleomagnetic data of ODP 758

In addition to containing discrete tephra layers, ODP 758 contains records of geomagnetic reversals and excursions – the relationships between the tephra and geomagnetic are quantifiable. For the purpose of this discussion/study we have focussed on the composite ODP 758 record (ODP 758A, 758B, 758C) as presented by Farrell and Janecek (1991) (Fig. 2). By constructing a composite depth section from Holes 758A and 758B it was possible to splice across recovery gaps with the result being an undisturbed, continuous sedimentary section that extends from 0 to 116 mbsf, which is equivalent to the past *c.* 7 Ma (well beyond the time interval of interest for this study). The continuity of this composite section was checked with several independent stratigraphies (e.g., Farrell and Janecek, 1991). The paleomagnetic data for ODP 758 are not ideal in that they were not collected from discrete samples; the U-channel and on-board measurements have in all probability

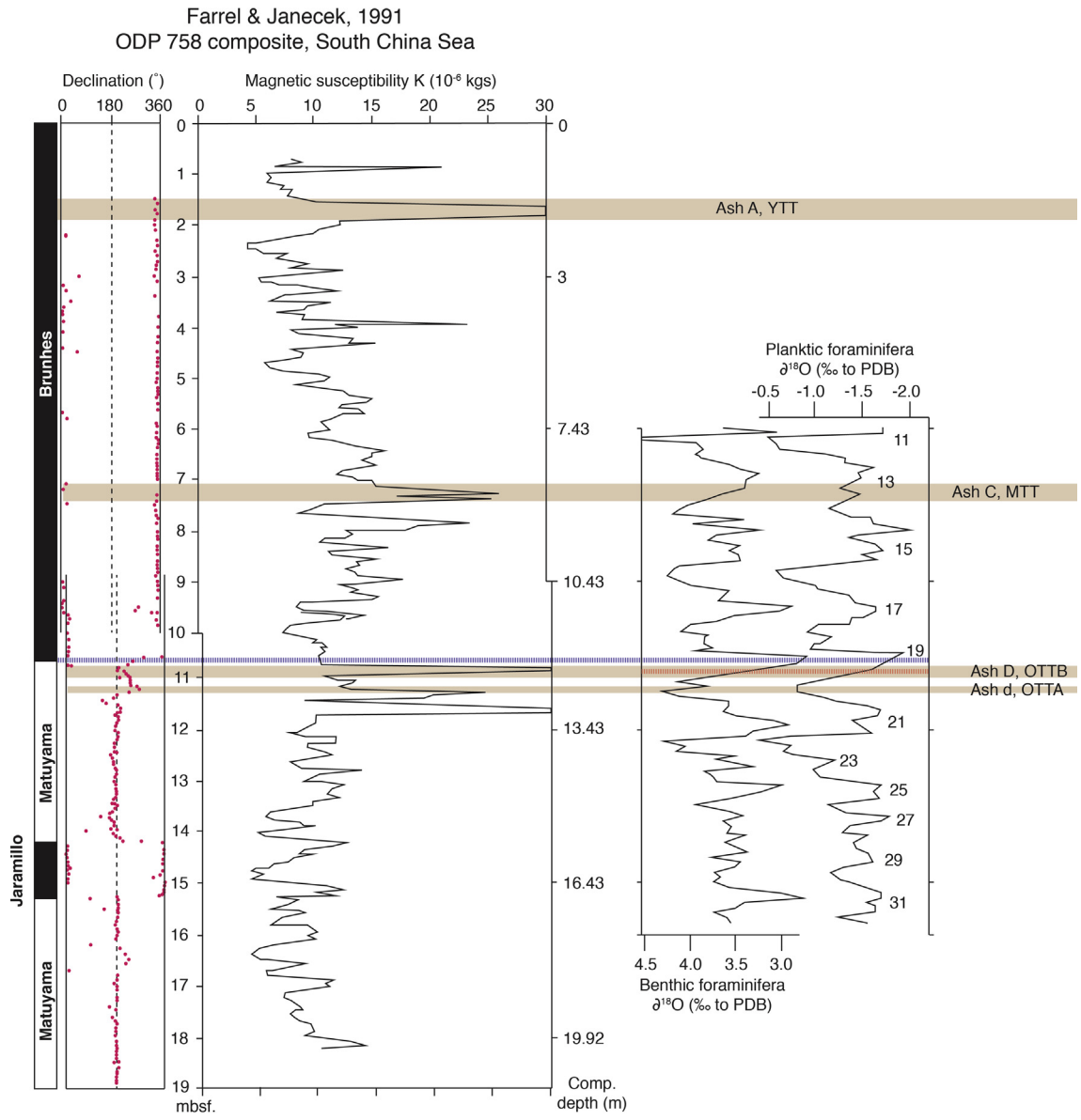

Fig. 2. Composite core for ODP 758 (Farrell and Janecek, 1991) showing (i) composite magnetic stratigraphy (declination) for ODP 758, (ii) Magnetic susceptibility for ODP 758 with the locations of the Ashes A, C, D and d (i.e., correlated Toba Tuffs), and (iii) the geomagnetic timescale. Planktic and Benthic foraminifera $\partial^{18}O$ records for ODP 758 composite are shown highlighting the position of the MBB within Marine Isotope Stage 19. The orange line (coincident with Ash D) shows the position of Termination IX within ODP 758. (For interpretation of the references to colour in this figure legend, the reader is referred to the web version of this article.)

smoothed the paleomagnetic signal, but the core still retains clear transition zones and paleomagnetic directional changes (Shipboard Scientific Party, 1989; Dehn et al., 1991; Farrell and Janecek, 1991; Gee et al., 1991).

1.5. The location of the MBB at site 758

Chen et al. (1995) determined an astronomical age of *c*. 784 ka for the MBB in ODP 758. Although similar to the MBB age of Shackleton et al. (1990) (780 ka) there is no uncertainty associated with these ages and as such, it is unclear whether the offset is 'real' (i.e., geological or methodological). However, it has been suggested that any astronomically tuned age for this period of time cannot be defined better than to within ± 5 ka due to uncertainties in the phase relationship between insolation and climate (Martinson et al., 1987; Imbrie and Imbrie, 1980). The tuning approach of Chen et al. (1995) did vary from that of Shackleton et al. (1990), whereas the latter tuned their $\partial^{18}O$ data to the model of Imbrie and Imbrie (1980) from 0 to 1.6 Ma, and to the obliquity cycles from 1.6 to 2.6 Ma, Chen et al. (1995) tuned their entire record to the ice volume simulation based on the model of Imbrie and Imbrie (1980). This approach allowed for a fine tuning approach of both the 41 and 23 ka cycles simultaneously.

The ODP 758 $\partial^{18}O$ data (also a composite of $\partial^{18}O$ measurements from ODP 758A and ODP 758B; Farrell and Janecek, 1991; Chen et al., 1995) show the location of the MBB in the early part of Marine Isotope Stage (MIS) 19 (Fig. 2), earlier than the position of the MBB as noted by Channell et al. (2010) in the North Atlantic. This is not uncommon; the MBB has been identified in the middle of MIS 19 (Suganuma et al., 2015), at the start of MIS 19 (Horng et al., 2002) and even within MIS 20 (Langereis et al., 1997), although the latter was attributed to delayed acquisition of the Earth's magnetic signal in the sediment (i.e., lock-in of paleomagnetic remanence) (Kent, 1973). As a consequence, two important questions emerge: (1)

should we expect the MBB to be globally located at the exact same location within a MIS? And (2) if so, why do we see such variation in the location of the MBB in different $\partial^{18}O$ records? We consider these to be questions of temporal and spatial resolution within records - we revisit this discussion below.

1.6. The Jaramillo geomagnetic excursion at site 758

The Jaramillo geomagnetic excursion (JGE) was a reversal of the geomagnetic field that occurred *c*. 1000 ka (Singer, 2014; Kissel et al., 2014) and is also preserved within ODP 758. It was a short-term reversal in the Matuyama reversed magnetic chronozone. Within ODP 758 the JGE_{onset} is dated at *c*. 1070 ka and the $JGE_{termination}$ at *c*. 997 ka (Chen et al., 1995). The Toba tephra are positioned above the JGE within ODP 758.

1.7. Australasian microtektites

Australasian microtektites have been found below the MBB within sediment cores from throughout the Indian Ocean, western equatorial Pacific Ocean, Philippine, Sulu and Celebes Seas, and most recently the South China Sea (Hyodo et al., 2011 and references within). The Australasian tektites have previously been dated by $^{40}Ar/^{39}Ar$ at 799.2 ± 3.4/3.8 ka (Smit et al., 1991) with the data of Yamei (2000) reproducing this age but suggesting the presence of excess ^{40}Ar (noted from isochron analysis of the data, Yamei 2000). As such, the current $^{40}Ar/^{39}Ar$ age for the Australasian microtektites should be considered as a maximum age constraint.

Within Site 758 the peak abundance of Australasian microtektites occurs 8 cm below a tephra horizon labelled as Ash 'D' and immediately prior to Termination IX (Lee et al., 2004). We know from other Pacific and Indian Ocean records that the Australasian Tektite peak concentration is located immediately prior to Termination IX (e.g., Glass and Koeberl, 2006; Valet et al., 2014), the transition from Marine Isotope Stage (MIS) 19–20. Despite a large degree of dispersion throughout the core, the Australasian Tektites main concentration peak is in the correct stratigraphic position relative to other cores from throughout the region.

1.8. ODP 758 and LR04

LR04 is a 5300 ka stack of $\partial^{18}O$ records from 57 globally distributed sites that have been aligned using an automated graphic correlation algorithm (Lisiecki and Raymo, 2005). This was the first Pliocene-Pleistocene stack to contain more than three records that extend back beyond 850 ka. The LR04 stack contains the composite ODP 758 core data. As an automated graphic correlation algorithm was used to construct the stack, its stratigraphic features are therefore independent of any time scale. An age model was subsequently constructed by aligning the benthic $\partial^{18}O$ stack to a simple model of ice volume whilst taking into consideration the average stacked sedimentation rate of the individual sediment cores. The LR04 stack places the MBB at *c*. 780 ka (following Shackleton et al., 1990).

2. Study scope

Using a combination of tephrochronology and high-precision $^{40}Ar/^{39}Ar$ geochronology we aim to examine the temporal relationship between the Toba tephra layers preserved in ODP 758 to primarily constrain the age of the MBB, the Australasian Tektites and Termination IX within the Indian Ocean. Furthermore, we examine the relationship of the MBB to the Bishop Tuff and Lava Creek Tuff B (LCTB) in North America. Our findings agree perfectly with those of Sagnotti et al. (2014) and further question the accuracy of the Channell et al. (2010) MBB age estimation, unless an 'extremely' diachronous reversal is invoked, an event that our data discount.

3. Field relations, proximal tuffs: Sumatra

Fieldwork was conducted on Sumatra to directly sample the relevant proximal (crystal-rich) Toba deposits. Samples were collected from roadside exposures from Siguragura and to the north of Haranggoal. Sample locations shown in Fig. 3 relative to the accepted stratigraphy of those sequences (Chesner and Rose 1991, Chesner et al., 1991). Correlation of proximal deposits across the caldera is extremely difficult because of poor exposure and abundant rainforest vegetation, but has been attempted previously by Knight et al. (1986) and Chesner et al. (1991).

3.1. Haranggoal (2° 52′ 39″ N, 98° 40′ 26″ E)

Toba eruptive units are intermittently exposed along the road that climbs the caldera wall to the northwest of Haranggoal. Andesitic lavas, dated at c. 1.3 Ma (Chesner et al., 1991), are exposed at the present lake level. The c. 1.2 Ma Haranggoal dacite tuff (HDT) overlies the andesitic lava flows (Chesner et al., 1991). The HDT is a brown, densely welded and often-jointed (radial and columnar) ignimbrite with large, lightly coloured, flattened pumices that reach 1 m in length (Chesner and Rose, 1991) and is exposed in the roadside to elvations of ~1060 m. Above the HDT are three further eruptive units (see Fig. 3). At elevations above about ~1250 m near Haranggoal, the YTT caps the eruptive sequence, as it does for almost all of the area surrounding Lake Toba. Below this, Chesner et al. (1991) $^{40}Ar/^{39}Ar$ dated a middle unit, 140 m-thick, to 501 ± 5 ka, noting that this had a normal paleomagnetic polarity, and ascribed this unit to the MTT. The light gray upper parts of the MTT (containing generally black and glassy fiamme), are underlain by a dark gray to black, often columnar-jointed vitrophyric tuff (up to 100 m thick) also normally magnetised (Knight et al., 1986). This vitrophyre has been described as the basal component of MTT by Chesner and Rose (1991). The vitrophyric unit underlying the light gray MTT does not resemble OTT deposits reported from elsewhere around the lake (e.g. Siguragura, see below) and for this reason previous authors have assumed that OTT is absent from this part of the caldera wall near Haranggoal. We now know that the dark vitrophyric underlying unit is not part of the MTT sequence, but is an older eruption product (discussed below).

3.2. Siguragura (2° 31′ 16.7″ N, 99° 16′ 29.2″ E)

Chesner and Rose (1991) described the Oldest Toba Tuff at Siguragura. The OTT is well exposed on the Uluan block and along the course of the Asahan River, SE of the lake, where it is a very thick (> 300 m in most locations) densely welded ignimbrite that is brown to light grey in colour. On the Uluan block OTT it is often columnar jointed and numerous flow units can be recognised, and contains fiamme (up to 30 cm, Chesner and Rose, 1991). The OTT sample used in this study was collected from Siguragura, in the Asahan River valley, and material from this area had been previously $^{40}Ar/^{39}Ar$ dated by Diehl (1987) (c. 840 ka) and noted to have a reversed paleomagnetic polarity.

4. Field relations, proximal tuffs: North America

4.1. Bishop Tuff

The Bishop Tuff has been described in detail by many other studies (e.g., Simon et al., 2014; Ickert et al., 2015) and hence here we just provide details of specific sampling sites. Three samples of

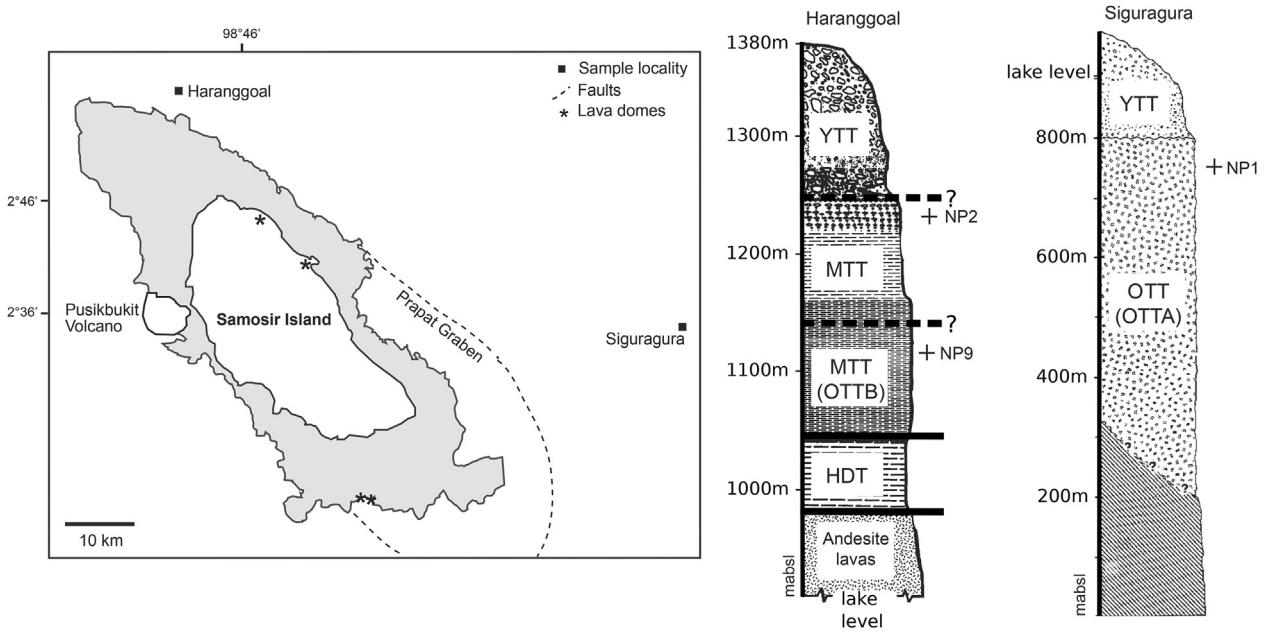

Fig. 3. Map showing the location of sampling sites relative to the Toba Caldera with the respective stratigraphies for both sites. Sample locations: NP9 (OTTB in this study) - 2° 53′ 13.9″ N, 98° 39′ 51.1″ E, 1115 m asl; NP2 (MTT) - 2° 52′ 48.9″ N, 98° 39′ 48.8″ E, 1230 m asl; NP1 (OTTA in this study) - 2° 31′ 09.6″ N, 99° 16′ 29.2″ E, 750 m asl. Further details on the stratigraphic sequences are provided in the text.

the Bishop Tuff, each representing distinct phases of the eruption, were sampled. Localities and ignimbrite subpackage designations (WH1997) refer to Wilson and Hildreth (1997). JIS09MLV33 (BR1): Near-vent facies in the Mono lobe. A single large pumice clast ~8000 cm^3 was collected from locality 208 in subpackage Ig2NWa (WH1997), at N 37°45.814′ latitude, W 118°59.836′ longitude. BR11-3: Fall deposit approximately 42 km from the vent in the Tableland lobe. Multiple pumice clasts from ~10 to 700 cm^3 were collected from locality 16/17 in subpackage Ig2E (WH1997), at N 37°27.578′ latitude, W 118°21.990′ longitude. BR11-4: Near-vent facies in the Gorges lobe. A single block of densely welded tuff ~3000 cm^3 was collected from near locality 444 in subpackage Ig1Eb (WH1997), at N 37°35.288′ latitude, W 118°42.284′ longitude.

4.2. Lava Creek Tuff B

Similarly, the Lava Creek Tuff B (LCTB) has been described in detail by many other studies (e.g., Wotzlaw et al., 2015) and as such, details of just the sampling site are described. The LCTB ignimbrite was sampled from the location described by Christiansen (2001) at the quarry near the east end of the dam at Grassy Lake Reservoir, just south of Yellowstone National Park (N44°13.074′, W110°81.417′). The sample was from the relatively crystal-rich densely welded basal vitrophyre of the ignimbrite. Bulk composition of this sample is identical to compositions of LCTB reported by Christiansen (2001).

5. Analytical methods

5.1. Electron microprobe glass and biotite geochemistry

Major element compositions of glass and biotite from both the proximal Toba deposits (YTT, MTT, OTT) and distal deposits (Ash layers A, C, d, D, E) were determined using a wavelength-dispersive JEOL 8600 electron microprobe (EMP) at the Research Laboratory for Archaeology and the History of Art, University of Oxford. The instrument was calibrated at 15 kV using a range of mineral standards. A low beam current (6 nA), and defocused (10 μm) beam were used to analyse individual glass shards. Single biotite crystals were analysed with a beam current of 15 nA, and a 5 μm beam. Peak counting times were 30 s for all elements except Na (10 s in glass and 20 s in biotite). The EMP calibration was verified using a range of reference glasses from the Max Planck Institut (Jochum et al., 2006) and minerals from the Smithsonian (Jarosewich et al., 1980). Totals of glass analyses were mostly >95% and normalized to 100% to account for variable secondary hydration. Biotite analytical totals were typically >92 wt.%. All raw analyses of the glass and biotite, and the reference materials are included in appendix file 'SF#1' (.pdf).

5.2. $^{40}Ar/^{39}Ar$ dating

A detailed sample preparation routine is discussed by Mark et al. (2010) but briefly: feldspars (sanidine) were separated after disaggregating, washing and sieving followed by magnetic and density separations and finally ultrasonic cleaning in 5% hydrofluoric acid for 5 min. Feldspars were handpicked under binocular microscope for analysis. Samples were irradiated in the CLICIT facility of the Oregon State University TRIGA reactor using the Alder Creek sanidine (Nomade et al., 2005) as a neutron fluence monitor.

$^{40}Ar/^{39}Ar$ analyses were conducted at the NERC Argon Isotope Facility, Scottish Universities Environmental Research Centre (SUERC) and the Berkeley Geochronology Center (BGC). Samples analyzed at BGC were run and reported blindly, without knowledge of the SUERC results (and vice versa). Details of irradiation durations, J measurements, discrimination corrections are provided in appendix file SF#3b (.pdf). Irradiation correction parameters are shown below.

For J determinations three bracketing standard positions

surrounding each unknown were used to monitor the neutron fluence. Ten measurements were made for each bracketing standard position. The weighted average $^{40}Ar^*/^{39}Ar_K$ was calculated for each well, and the arithmetic mean and standard deviation of these three values was used to characterize the neutron fluence for the unknowns. This approach was deemed sufficient as, due to the relatively short irradiation durations, there was no significant variation between the three positions in a single level of the irradiation holder. This also facilitated high-precision measurement of the J-parameter. Note that for all J-measurements no data were rejected.

Samples were analyzed in several batches; backgrounds and mass discrimination measurements (via automated analysis of multiple air pipettes) specific to each batch are summarized in appendix file 'SF#1' (.pdf). Air pipettes were run (on average) after every 5 analyses. Backgrounds subtracted from ion beam measurements were arithmetic averages and standard deviations. Mass discrimination was computed based on a power law relationship (Renne et al., 2009) using the isotopic composition of atmospheric Ar reported (Lee et al., 2006) that has been independently confirmed (Mark et al., 2011). Corrections for radioactive decay of ^{39}Ar and ^{37}Ar were made using the decay constants reported by Stoenner et al. (1965) and Renne and Norman (2001), respectively. Ingrowth of ^{36}Ar from decay of ^{36}Cl was corrected using the $^{36}Cl/^{38}Cl$ production ratio and methods of Renne et al. (2008) and was determined to be negligible. Argon isotope data corrected for backgrounds, mass discrimination, and radioactive decay and ingrowth are given in the appendix file 'SF#1' (.pdf).

At SUERC the samples were analyzed by total fusion and step-heating with a CO_2 laser and measurements made using a MAP 215-50 (MAP2) noble gas mass spectrometer. The mass spectrometer is equipped with a Nier-type ion source and analogue electron multiplier detector. Mass spectrometry utilized peak-hopping by magnetic field switching on a single detector in 10 cycles.

At BGC the samples were analyzed by total fusion with CO_2 lasers on two different extraction systems mated to MAP 215 mass spectrometers (MAP1 and MAP3). MAP1 is a 215C and MAP3 is a 215-50. Both have Nier-type ion sources and analog electron multiplier detectors. Mass spectrometry utilized peak-hopping by magnetic field switching on a single detector in 10–15 cycles.

Ages were computed from the blank-, discrimination- and decay-corrected Ar isotope data after correction for interfering isotopes based on the following production ratios, determined from fluorite and Fe-doped $KAlSiO_4$ glass: $(^{36}Ar/^{37}Ar)_{Ca} = (2.650 \pm 0.022) \times 10^{-4}$; $(^{38}Ar/^{37}Ar)_{Ca} = (1.96 \pm 0.08) \times 10^{-5}$; $(^{39}Ar/^{37}Ar)_{Ca} = (6.95 \pm 0.09) \times 10^{-4}$; $(^{40}Ar/^{39}Ar)_K = (7.3 \pm 0.9) \times 10^{-4}$; $(^{38}Ar/^{39}Ar)_K = (1.215 \pm 0.003) \times 10^{-2}$; $(^{37}Ar/^{39}Ar)_K = (2.24 \pm 0.16) \times 10^{-4}$, as determined previously for this reactor in the same irradiation conditions (Renne, 2014). Ages and their uncertainties are based on the methods of Renne et al. (2010), the calibration of the decay constant as reported by Renne et al. (2011) and the ACs optimization age (1.1891 ± 0.0009 Ma, R^{ACs}_{FCs}: 0.041707 ± 0.000011, 1 sigma) as reported by Niespolo et al. (2016), except where noted. The optimization-modeled age for the ACs standard has accurate quantifiable uncertainties and hence is favored here over the astronomically tuned ACs age presented by Niespolo et al. (2016). The reason for this is that the astronomical calibration has unknown uncertainty and confidence intervals and uses best guess 'assumptions' to constrain, for example, phase relationships between insolation and climate within the Pleistocene.

For some of the age comparisons made herein, contributions from sources of systematic uncertainty (i.e., uncertainties in $^{40}Ar/^{4}K$ of the standard and ^{4}K decay constants) are neglected and only analytical uncertainties in isotope measurements of samples and standards are included. These uncertainties are referred to herein as "analytical precision". For the purposes of this study analytical uncertainties include contributions from uncertainties in the interference corrections because these interference corrections have variable effects due to the slight variable chemistry of the samples considered. Where not otherwise distinguished, uncertainties are stated as X ± Y/Z, where Y is the analytical uncertainty as defined above, and Z is the full external precision considering both analytical and systematic sources of uncertainty (e.g., decay constant).

Age computation uses the weighted (by inverse variance) mean of $^{40}Ar^*/^{39}Ar_K$ values for the sample and standard, combined as *R*-values and computed using the method of Renne et al. (2010). Outliers in both single-crystal samples and standards were discriminated using a 3-sigma filter applied iteratively until all samples counted are within 3 standard deviations of the weighted mean ± one standard error. This procedure screened older crystals that are logically interpreted as xenocrysts. No younger outliers were recorded during analysis of all samples. Processing of the data using the *n*MAD approach of Kuiper et al. (2008) has no impact on the probability distribution plots for each sample.

The analytical approach adopted was to initially analyze at all times single crystals of sanidine by total fusion (SUERC & BGC). Following the initial analyses if no xenocrystic contamination was observed, samples of small crystal populations (*n*3) were step-heated (SUERC). The purpose of the step heating was to verify that initial trapped $^{40}Ar/^{36}Ar$ compositions overlap with accepted atmospheric values (Lee et al., 2006; Mark et al., 2011).

6. Results

6.1. Fieldwork & tephra geochemistry

There are limited accessible outcrops around Lake Toba that preserve a full volcanic stratigraphy. Hence the eruption history of Toba has been pieced together from distal locations (e.g., marine cores) and a couple of non-correlated sites located proximal to the caldera. As discussed above, we sampled the deposits at two of these key localities, Haranggoal at Siguragura (Fig. 3), as the volcanic units preserved at these localities have been previously ascribed to the three different Toba eruptions (OTT, MTT and YTT). At Siguragura the OTT unit is unconformably overlain by the YTT. The YTT is also preserved at Harrangoal and is underlain by two units ascribed to the MTT, which lie above the Harrangoal Dacitic Tuff (HDT, Shane et al., 1995; Lee et al., 2004, Chesner and Rose, 1991). Although the lowermost vitrophyric portion of the unit between YTT and HDT lies within the same stratigraphic position as OTT, it was assumed by Chesner and Rose (1991) to be the MTT, as it appears texturally different from the OTT at Siguragura.

Interestingly, within ODP 758 there are two tephras of the approximate age of the OTT, Ash d and Ash D. We hypothesized that the OTT deposits at Siguragurra and Harrangoal are products of two different eruptive events that occurred *c*. 800 ka, which correspond to Ash D (*termed* OTTB, Haranggoal) and Ash *d* (*termed* OTTA, Siguragura) in the distal ODP 758 core. Our geochemical data on both glass and biotite (Fig. 4) show that despite a different appearance, this lower presumed MTT unit at Haranggoal is compositionally indistinguishable from the other OTT proximal deposits and that indeed Ash d and Ash D correspond to two different eruptions that occurred about the same time as 'the OTT'

(hence labelling OTTA and OTTB). Based upon the previously published estimated sedimentation rate in ODP 758 of 1.7 cm/ka (Farrell and Janecek, 1991), there would be *c.* 6 ka between Ash *d* and Ash D.

6.2. $^{40}Ar/^{39}Ar$ dating results

All of our new $^{40}Ar/^{39}Ar$ data are presented in Figs. 5–8. Pooled ages for the two samples dated by both SUERC and BGC are calculated from the weighted mean *R*-values (Renne et al., 1998) corresponding to the single crystal total fusion measurements for each sample. All data are presented at the 1 sigma confidence level and are summarized in Table 1.

OTTA$_{total\ fusion\ (pooled)}$: SUERC analysed 61 crystals and BGC analysed 40 crystals (sample NP1). One data point was rejected due to the analysis of a plagioclase grain rather than a sanidine crystal. Data define a weighted mean pooled age of 792.5 ± 0.5/0.6 ka (Fig. 5).

OTTA$_{step\text{-}heating}$: SUERC performed four step-heating experiments on four different aliquots of sanidine crystal populations (*n*3) (sample NP1). All experiments yielded 100% ^{39}Ar plateaux with initial $^{40}Ar/^{36}Ar$ trapped components that overlapped with atmospheric values (Lee et al., 2006). The weighted mean plateau age (791.9 ± 1.0/1.1 ka) and inverse isochron age (Fig. 6) are indistinguishable at the 1 sigma level from the total fusion weighted mean age.

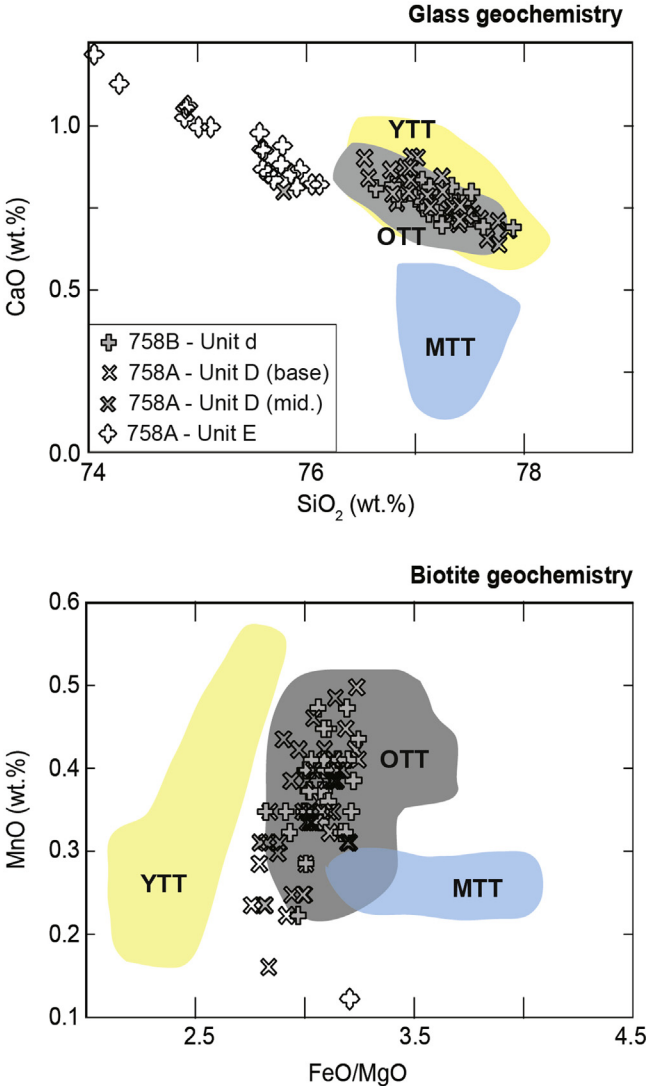

Fig. 4. Glass major element and biotite geochemistry for ODP 758 Ashes D, d and E as well as proximal YTT, MTT and OTT data from Siguragura and Harrangoal. Note the glass major element geochemistry cannot distinguish between the YTT and OTT deposits, but the biotite shows a definitive correlation with the OTT. Ash E was distinctly lacking in biotite, only one crystal was found. Data fields from Smith et al. (2011).

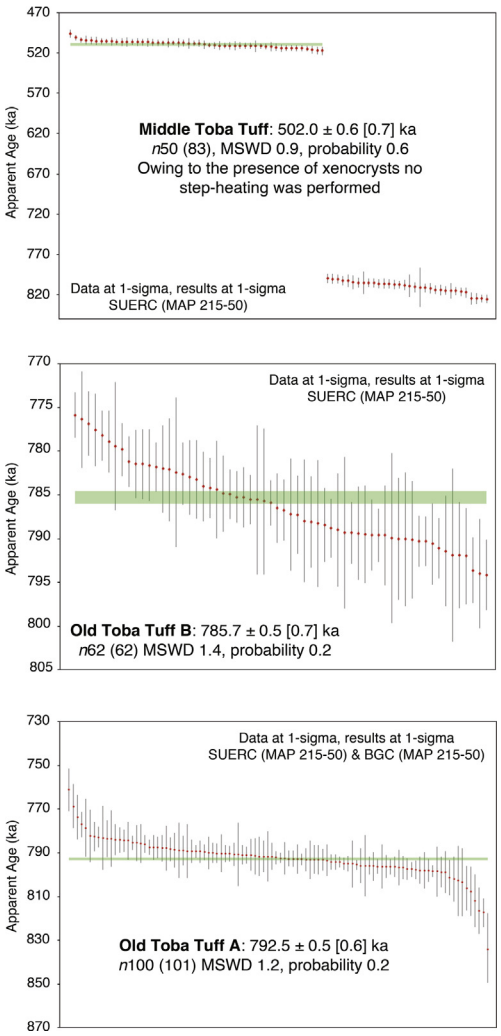

Fig. 5. $^{40}Ar/^{39}Ar$ single crystal fusion data for the MTT, OTTA and OTTB.

OTTB$_{total\ fusion}$: SUERC analysed 62 crystals of OTTB (sample NP9). Data define a weighted mean age of 785.7 ± 0.5/0.7 ka (Fig. 5). No data points were rejected from the age calculation.

OTTB$_{step\text{-}heating}$: SUERC performed four step-heating experiments on four different aliquots of sanidine crystal populations (*n*3) (sample NP9). All experiments yielded 100% ^{39}Ar plateaux with initial $^{40}Ar/^{36}Ar$ trapped components that overlapped with atmospheric values (Lee et al., 2006). The weighted mean plateau age (785.3 ± 0.8/1.0 ka) and inverse isochron age (Fig. 6) are indistinguishable at the 1 sigma level from the total fusion weighted mean age.

MTT$_{total\ fusion}$: SUERC analysed 83 crystals of MTT sanidine (sample NP2). The data show a bimodal distribution with an older age population of *c.* 800 ka (*n*33) and a juvenile population defining an age of 502.0 ± 0.6/0.7 ka (*n*50) (Fig. 5). We consider the statistically significant juvenile population to define the age of the MTT eruption. Owing to the presence of xenocrysts we did not perform

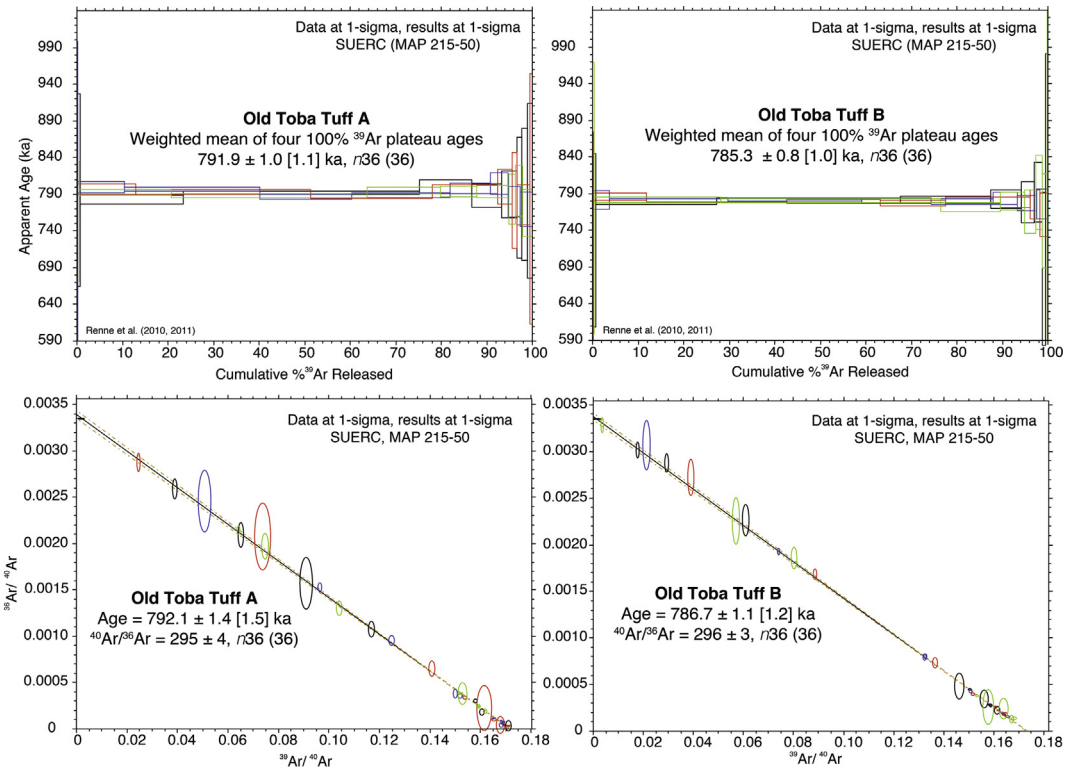

Fig. 6. Incremental step-heating $^{40}Ar/^{39}Ar$ age spectra and isotope correlation plots (OTTA and OTTB).

incremental step-heating on small crystal populations. Note the xenocryst age population is consistent with the approximate age of the OTT.

$BT_{total\ fusion}$: SUERC analysed 225 crystals of BT sanidine using a single mass spectrometer and BGC analysed 94 crystals using two different mass spectrometers with the samples irradiated in two separate batches. The data yielded a weighted pooled mean of 766.8 ± 0.4/0.6 ka (*n*319), with no data points rejected (Fig. 7).

$BT_{step\text{-}heating}$: SUERC performed eight step-heating experiments on eight different aliquots of sanidine crystal populations (*n*3). All

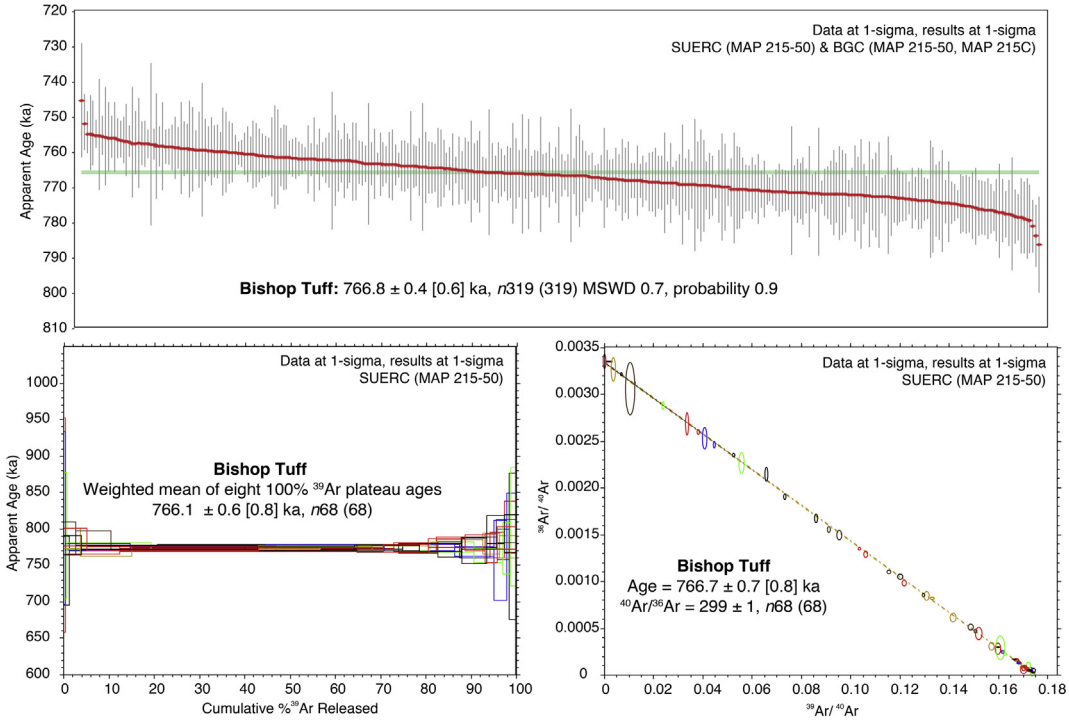

Fig. 7. $^{40}Ar/^{39}Ar$ single crystal fusion data and incremental step-heating age spectra and isotope correlation plots for Bishop Tuff sanidine.

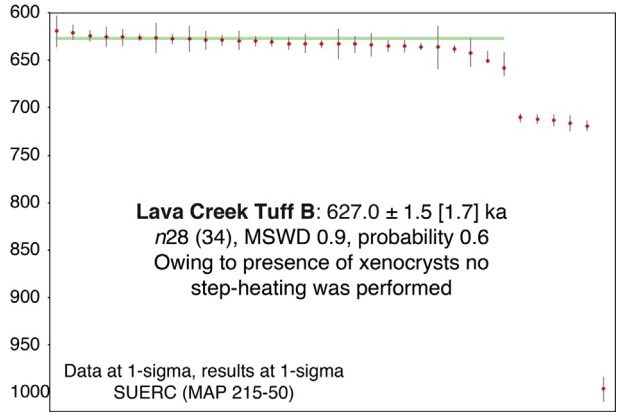

Fig. 8. $^{40}Ar/^{39}Ar$ single crystal fusion data for LCTB.

experiments yielded 100% ^{39}Ar plateaux with initial $^{40}Ar/^{36}Ar$ trapped components that overlapped with atmospheric values (Lee et al., 2006). The weighted mean plateau age (766.1 ± 0.6/0.8 ka) and inverse isochron age (Fig. 7) are indistinguishable at the 1 sigma level from the total fusion weighted mean age.

LCTB$_{total\ fusion}$: SUERC analysed 34 sanidine crystals of LCTB. The data show a dominantly bimodal distribution with an older age population of *c*. 700 ka (*n*5) and a single old crystal of *c*. 960 ka (*n*1). 28 sanidine crystals defined a juvenile age population with weighted mean age of 627.0 ± 1.5/1.7 ka (Fig. 8). We consider this juvenile age population to define the age of the LCTB eruption. Owing to the presence of xenocrysts we did not perform incremental step-heating experiments.

The *R*-values and their corresponding ages (calculated weighted averages for samples that have both fusion age and step-heating age data) are shown in Table 1 and appendix file 'SF#1' (.pdf). It is these ages (Table 1) and associated *R*-values that are discussed throughout the remainder of the text.

7. Discussion

7.1. $^{40}Ar/^{39}Ar$ dating of the proximal Toba Tuffs

We performed $^{40}Ar/^{39}Ar$ dating on sanidine separated from the proximal YTT, MTT, OTTA (Siguragura) and OTTB (Harrangoal) that have been correlated geochemically to tephra layers preserved within the marine core record to construct a high-precision radioisotopic chronology for the Pleistocene of ODP 758 that is independent of the astronomical age model.

The $^{40}Ar/^{39}Ar$ age data for the YTT (Ash A) have been published previously and define a robust inverse isochron age, the data being reported relative to the ACs standard age of 1.2056 Ma (Renne et al., 2011). This age for the YTT was indistinguishable from the YTT age of Storey et al. (2012), relative to the same $^{40}Ar/^{39}Ar$ calibration. Taking the new published optimisation model ACs age of Niespolo et al. (2016) into account, we have taken this opportunity to recalculate the ages of Mark et al. (2013, 2014) and Storey et al. (2012). This yields the most accurate and precise age for the YTT, integrating the data from both laboratories to give an age of 73.7 ± 0.3/0.4 ka (R^{YTT}_{ACs}: 0.06196 ± 0.00025). Note the recalculated data is available in appendix file 'MBB data summary' (.pdf). The age of the MTT (502.0 ± 0.6/0.7 ka, R^{MTT}_{ACs}: 0.42219 ± 0.00050) is in agreement with the $^{40}Ar/^{39}Ar$ age of Chesner et al. (1991) allowing for differences in the $^{40}Ar/^{39}Ar$ calibration used. Our data for the OTT show that at *c*. 800 ka there were two temporally distinct eruptions from the Toba volcano: OTTA and OTTB, 792.4 ± 0.5/0.6 ka (R^{OTTA}_{ACs}: 0.6646 ± 0.00042) and 785.6 ± 0.7/0.8 ka (R^{OTTB}_{ACs}: 0.66075 ± 0.00059), respectively. There is a *c*. 6 ka temporal offset between these two eruptions, which broadly agrees with the temporal offset suggested by the application of the average ODP 758 sedimentation rate between Ash *d* and Ash D (discussed above). The age for Ash D is also indistinguishable from the astronomically tuned age presented by Lee et al. (2004) of 788.0 ± 2.2 ka. These two ages (our $^{40}Ar/^{39}Ar$ age and the astronomically calibrated age) are in good agreement with the previous OTT/Ash D $^{40}Ar/^{39}Ar$ age of Hall and Farrell (1995) but younger than the OTT $^{40}Ar/^{39}Ar$ age of Diehl (1987).

The geochronological data and reinterpretation of the field geology show that the proximal Toba stratigraphy requires further detailed mapping, geochemistry, and eruption volume estimates so that we can develop a revised understanding of the old Toba eruption cycle. Ash E in ODP 758 is geochemically distinct from any of the Toba eruption products that we have analysed and, at present, the tephra provenance is unknown.

7.2. A Bayesian $^{40}Ar/^{39}Ar$ age-depth model for the Pleistocene of ODP 758

Bayesian age-depth modelling of ODP 758 was performed using the OxCal (ver. 4.2) software of Bronk Ramsey (2013) and Bronk Ramsey et al. (2013). A 'P_Sequence' (i.e., Poisson process) deposition model was applied (Bronk Ramsey, 2008), whereby the deposition rate of the sediment sequence is allowed to vary from that of a constant deposition rate through time (i.e., a uniform 'U_Sequence' in OxCal) according to the additional constraint of a parameter, 'k' (a higher value of k gives an increasingly linear deposition rate; lower values of k allow increasing flexibility away from a uniform deposition rate). In the context of sediment deposition, the P_Sequence model provides a realistic representation of sediment accumulation, with the complexity (randomness) of the underlying deposition modelled according to a Poisson process. The k parameter is not fixed *a priori*, allowing the program itself to determine an unbiased measure of the rigidity of the deposition rate, based upon the dating ('likelihood') information combined within the P_Sequence model prior (Bronk Ramsey and Lee, 2013).

Since the four tephra layers within ODP 758 represent macroscopic, instantaneous deposits ('instantaneous' in the context of the timescales considered here, at least), their respective thicknesses (Ash A, YTT 34 cm; Ash V, MTT 23 cm; Ash d, OTTB 13 cm; and Ash D, OTTA 2 cm thick) were excluded to provide an 'event-free depth' scale (e.g., Katsuta et al., 2007; Schlolaut et al., 2012) so that the regular, 'background' deposition rate could be effectively modelled.

In addition to the four $^{40}Ar/^{39}Ar$ dated tephra units, 'Date' functions were also inserted within the model to provide posterior age distributions for the depths of the MBB, Australasian tektite layer, and Jaramillo event (onset and termination) within ODP 758 (unlike the tephra units, these latter Date functions were included without any prior chronological information associated with them). The top and bottom of the sediment sequence (at 0 and 18.9 m depth) were additionally constrained by 'Boundary' functions, with

Table 1
Summary of $^{40}Ar/^{39}Ar$ ages and R-values for various samples.

	ODP 758	Age (Ma)	±1s (analytical)	±1s (full)	R	± 1s
OTTA	Ash d	0.79238	0.0005	0.0006	0.66646	0.00042
OTTB	Ash D	0.78559	0.0007	0.0008	0.66075	0.00059
MTT	Ash C	0.50200	0.0006	0.0007	0.42219	0.00050
YTT[a]	Ash A	0.0737	0.0003	0.0004	0.06196	0.00025
LCTB	N/A	0.62700	0.0015	0.0017	0.52734	0.00126
BT	N/A	0.76655	0.0004	0.0005	0.64473	0.00034

[a] Age recalculated from Storey et al., 2012; Mark et al., 2014 - Young Toba Tephra.

the upper boundary defined as the date of core extraction, AD 1988. The lower boundary was somewhat arbitrary, but represents the subsequent break between core sections below the Jaramillo event, the base of section 758B-2H (Shipboard Scientific Party, 1989). As there was no other sedimentological evidence within the stratigraphy for abrupt changes in the mode of sediment deposition, no further 'Boundary' functions were inserted within the P_Sequence model.

To assess whether two age distributions are statistically different within OxCal, the 'Difference' function (which simply subtracts one age distribution from another) is applied. Here, Difference queries were applied between the modelled ODP 758 ages and published ages for both the MBB and Australasian tektite layer. If the calculated probability range for the Difference query does not include zero at a given confidence level (typically, 95.4% confidence), a null hypothesis (that the two age distributions are consistent) can be rejected, and the ages can be described as being statistically significantly different (Macken et al., 2013; Wood et al., 2014).

Due to the limited number of likelihood data (i.e., four $^{40}Ar/^{39}Ar$ ages plus date of core extraction) within the model, there is no contradictory information (given the model prior) to 'pull' the modelled age-depth profile away from the raw, un-modelled data. Accordingly, all of the individual modelled data points exhibit excellent agreement indices of 100% (i.e., there is no evidence of stratigraphic inversions, or unreliable $^{40}Ar/^{39}Ar$ measurements.)

In order for the Poisson process (P_Sequence) age-depth profile to pass through these data points (which fall well away from linear sediment deposition), however, the modelled k parameter must be fairly low. The result of this is that the chronological precision of the interpolated (and extrapolated) depths is lower than if the deposition rate were more linear (i.e., if OxCal had determined a higher value for k). This reduction of modelled chronological precision becomes more pronounced further away from the $^{40}Ar/^{39}Ar$-dated core depths, as illustrated in Fig. 9.

Table 2 provides a summary of unit/event depth information (both mbsl and 'event-free' depth) used in the model construction. Note that interpretation of the positions of geomagnetic events within marine cores can be subjective - we have used the depths for the tephra layers and geomagnetic polarity reversals that have been published previously (Dehn et al., 1991; Farrell and Janecek, 1991). We note that, unfortunately, paleomagnetic intensity data are not available for ODP 758 but, due to the sensitivity of the model to the $^{40}Ar/^{39}Ar$ data and large uncertainties as we move away from these tie points, small changes (i.e., cm-scale changes) in the location of the MBB will not significantly impact the age ranges reported relative to the uncertainty associated with each modelled age (median age shifts approximately 0.7 ka/cm).

7.3. ODP 758 defined MBB age

The modelled age for the MBB (all modelled ages below reported at the 68.2% confidence level) is 784 ± 2 ka (Fig. 9). The MBB age as defined by ODP 758 is statistically older (at the 95.4% confidence level) than the proposed age of Channell et al. (2010) for the North Atlantic, but in complete agreement with the age proposed by Sagnotti et al. (2014) for samples from the Sulmona Basin. This age is indistinguishable from the ODP 758 astronomically tuned age of c. 784 ka.

7.4. ODP 758 defined JGE age

The modelled age range for the MBB is more precise than the extrapolated ages derived for the JGE_{onset} (median: 1082 ka, 1001–1159 ka) and $JGE_{termination}$ (median: 1002 ka, 933-1064 ka) (Fig. 9). This is due to the lack of an age constraint stratigraphically below the JGE within ODP 758 to anchor the Bayesian age-depth model. We are surprised however that even with absence of this constraint, that the median ages are relatively close to the reported ages for the onset (1070 ka) and termination (997 ka) of the JGE, respectively (Chen et al., 1995). With respect to current discussions in the literature (e.g., Singer, 2014) our data, owing to this low precision output from the model (i.e., lack of a temporal marker below the JGE_{onset}), do not advance understanding of the timing of the JGE.

7.5. The age of the Bishop Tuff

A robust age for the BT will allow determination of a North American MBB age that provides an independent comparison with the ODP 758 constraint. New data collected here and re-calculation of previously published data (e.g., Simon et al., 2014) shows that there is temporal alignment between the $^{40}Ar/^{39}Ar$ and ^{238}U-^{206}Pb geochronometers for the BT. However, we suggest caution in the (over)interpretation of the high precision zircon ID-TIMS ^{238}U-^{206}Pb ages for dating of Pleistocene volcanic eruptions.

A 'high-precision' BT zircon ID-TIMS ^{238}U-^{206}Pb age of 767.1 ± 0.5 ka (1 sigma, full uncertainty, Crowley et al., 2007) is significantly younger than the BT zircon ion microprobe (SIMS) ages (Reid and Coath, 2000; Simon and Reid, 2005) that suggest a mean pre-eruptive zircon magma residence time greater than 50 ka. Recently, Ickert et al. (2015) collected new SIMS and ID-TIMS ^{238}U-^{206}Pb age data and demonstrated both inter- and intra-grain variability in apparent U-Pb ages of BT zircon crystals. The new data support the forward modelling of Simon et al. (2008) and explain the discrepancy when interpreting the previous SIMS and ID-TIMS U-Pb age data (Reid and Coath, 2000; Simon and Reid, 2005; Crowley et al., 2007), but highlight that the single coherent population of juvenile crystals dated by Crowley et al. (2007) was not an 'eruption age' as previously implied, but a result of the strong correlation of the uncertainty in one component of the ^{230}Th disequilibrium correction. If the correlation is accounted for correctly then there exists substantial variability in the ages of the zircon crystals that precludes determination of a meaningful weighted mean crystallisation age.

The dating of BT zircon by U/Pb methods is highly challenging because the concentration of radiogenic Pb is low and the correction required for disequilibrium in the intermediate daughter products is large. These corrections for young zircon are significant, for example, a correction of greater than 80 ka was employed previously for BT zircon (Crowley et al., 2007). Moreover, the corrections are often based on best-case scenarios and assumptions (models) that are difficult to validate, e.g., that the host magma 'Th/U_{melt}' composition employed accurately represents the melt composition from which the zircon grew and requires that the magma itself was in U-series equilibrium prior to zircon growth. Hence the utmost caution must always be employed when interpreting geologically young ID-TIMS ^{238}U-^{206}Pb BT zircon data with respect to 'eruption ages' and we suggest that in general, such ages reported with relative uncertainties at the permil level are suspect of being unduly optimistic.

Several studies have now shown that young ID-TIMS ^{238}U-^{206}Pb zircon ages 'approach' eruption ages (e.g., Rivera et al., 2013), but as highlighted by Ickert et al. (2015) - when interpreting such data (i.e., zircon that forms/closes over a continuum rather than in response to a specific geological event, e.g., eruption) one should appreciate that employment of a weighted mean to geologically young high-precision zircon ages requires an assumption that necessitates a geologically implausible event. A further, important point to note is how the Th/U_{melt} uncertainty is propagated in the

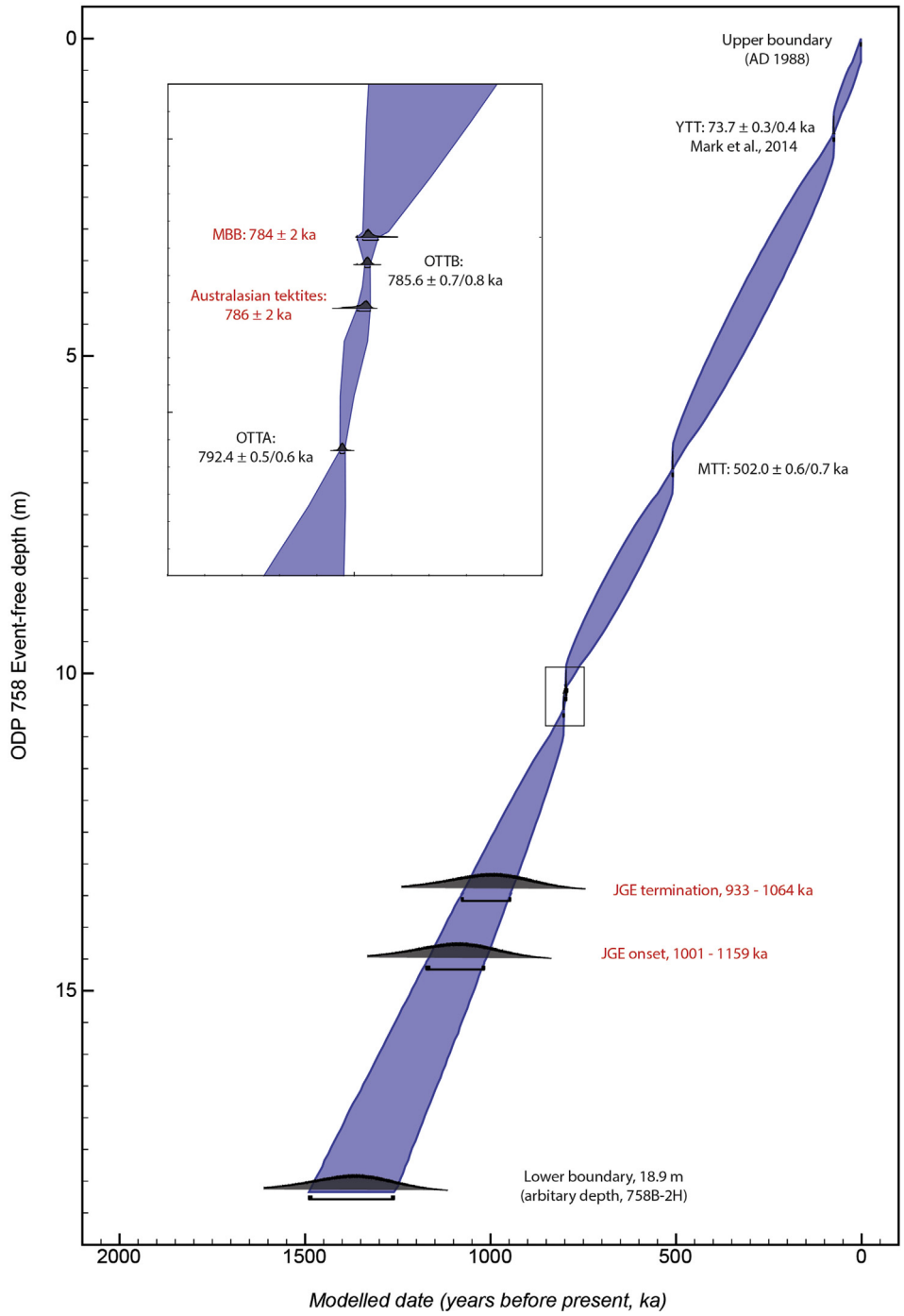

Fig. 9. Bayesian age-depth model for ODP 758. Anchor points shown in black and model outputs shown in red. The horizontal bars beneath each probability distribution, and the interpolated blue probability envelope represent the 68.2% confidence level. (For interpretation of the references to colour in this figure legend, the reader is referred to the web version of this article.)

correction (e.g., Crowley et al., 2007). This also affects the reported uncertainty of the new zircon rim 'eruption age' measured by SIMS (Chamberlain et al., 2014; discussed in-depth by Ickert et al., 2015). For the uncertainty propagation two approaches are prevalent. The first is similar to that of Crowley et al. (2007). The Th/U_{melt} correction is applied to each individual zircon analysis and then the weighted mean of the population is determined. In the second the Th/U_{melt} is treated as a systematic variable, and so this uncertainty is propagated following determination of a weighted mean age, applying it to the weighted mean $^{206}Pb^*/^{238}U$. The latter leads to a larger and we contend a more realistic age uncertainty. Note that the uncertainty on the corrected age has an inverse relationship with the Th/U_{melt} value, which is clearly demonstrated in Fig. 10.

Sarna-Wojcicki et al. (2000) presented the first 'high-precision' $^{40}Ar/^{39}Ar$ age measurements from the BT but recently the BT has been extensively studied. Rivera et al. (2011) reported an $^{40}Ar/^{39}Ar$ sanidine age of 767.4 ± 1.1 ka (R^{BT}_{FCs}: 0.02706 ± 0.00005), relative to their proposed astronomically tuned age for Fish Canyon sanidine (FCs). Zeeden et al. (2014) made measurements in the same laboratory and reported a BT $^{40}Ar/^{39}Ar$ age that is identical to the age

Table 2
Constraints used in Bayesian modelling (depths provided as mbsl, see Fig. 2 for composite scale).

	Core sampled	Thickness (cm)	Depth (mbsf)	Peak abundance depth (mbsf)	Reference	Geochem. Correlation (glass & biotite)
Ash A	ODP 758 1H	34	1.50–1.84		Dehn et al., 1991	YTT
Ash C	ODP 758 2H	23	7.12–7.35		Dehn et al., 1991	MTT
Ash D	ODP 758 2H	13	10.80–10.93		Dehn et al., 1991	OTTB (Haranggoal)
Ash d	ODP 758 2H	2	11.25–11.27		Dehn et al., 1991	OTTA (Siguragura)
Ash E	ODP 758 2H	5	11.62–11.67		Dehn et al., 1991	?
MBGR			10.75		Farrell & Janecek, 1991	
$JGE_{termination}$			14.2		Farrell & Janecek, 1991	
JGE_{onset}			15.28		Farrell & Janecek, 1991	
Australasian tektites		63	10.93–11.56	11.01	Lee et al., 2004	

reported by Rivera et al. (2011) but note they rejected more than 30% of their data culling the MSWD to 0.3 to improve analytical precision. Although the data were trimmed symmetrically around the determined mean (not impacting accuracy), this is an approach that is not 'best practice' with respect to statistical assessment of geochronological data. Relative to the highest precision attainable using the $^{40}Ar/^{39}Ar$ technique, the data of Sarna-Wojcicki et al. (2000), Rivera et al. (2011) and Zeeden et al. (2014) can be improved on. Thus we collected new high-precision $^{40}Ar/^{39}Ar$ age data to better define R^{BT}_{ACs} (Fig. 7). Exhaustive new analyses validate the results of Rivera et al. (2011) and Zeeden et al. (2014). However, for calculation of $^{40}Ar/^{39}Ar$ ages we do not favour the use of the FCs calibration presented by Rivera et al. (2011); we provide our reasoning below.

$^{40}Ar/^{39}Ar$ data (Renne et al., 2013) for the Cretaceous-Palaeogene (K-Pg) boundary show that the orbitally-tuned FCs calibration of Rivera et al. (2011) places the K-Pg boundary exactly intermediate between two possible choices of 405 ka orbital eccentricity cycles. The implication is that the astronomically tuned age for FCs (Rivera et al., 2011) is paradoxically inconsistent with any astronomically tuned age for the K-Pg boundary. Rather the $^{40}Ar/^{39}Ar$ calibration (FCs age) of Renne et al. (2011) is proven to be the most consistent with the orbitally-tuned age (Kuiper et al., 2008) for the K-Pg boundary (Renne et al., 2013). It is this calibration with robust and quantifiable uncertainties that we favour. Using the updated R^{ACs}_{FCs} (0.041707 ± 0.000011) reported by Niespolo et al. (2016) as a parameter in the optimized calibration of Renne et al. (2010), along with the decay constant from Renne et al. (2011), our $^{40}Ar/^{39}Ar$ data define a BT eruption age of 766.6 ± 0.4/0.5 ka (R^{BT}_{ACs}: 0.64473 ± 0.00034) (Fig. 7).

In view of our comprehensive data set, from multiple eruptive BT units (*n*3), laboratories (*n*2), mass spectrometers (*n*3), and operators (*n*3), we regard this as the most precise and accurate age for the BT. The $^{40}Ar/^{39}Ar$ age of Rivera et al. (2011) recalculated relative to the same parameters as our data is 767.6 ± 1.0/1.1 ka, the $^{40}Ar/^{39}Ar$ age of Sarna-Wojcicki et al. (2000) is 768.7 ± 3.2/3.3 and the $^{40}Ar/^{39}Ar$ age of Simon et al. (2014) is 769.0 ± 3.1/3.2 ka. These data are all indistinguishable relative to each other and consistent with a relatively imprecise astronomically tuned age for the Bishop Tuff of 765 ± 8 ka (Zeeden et al., 2014). The data are also consistent with the interpretation of Ickert et al. (2015) that the BT zircon ID-TIMS ^{238}U-^{206}Pb eruption age is < 775 ka. Fig. 11 shows a summary of these data against the 'weighted mean' BT zircon ID-TIMS ^{238}U-^{206}Pb age (Crowley et al., 2007) and the BT zircon ID-TIMS ^{238}U-^{206}Pb age distribution of Ickert et al. (2015).

The ^{238}U-^{206}Pb data, $^{40}Ar/^{39}Ar$ and astronomical ages have all converged for the BT, to provide a robust temporal marker for the Pleistocene Time Scale.

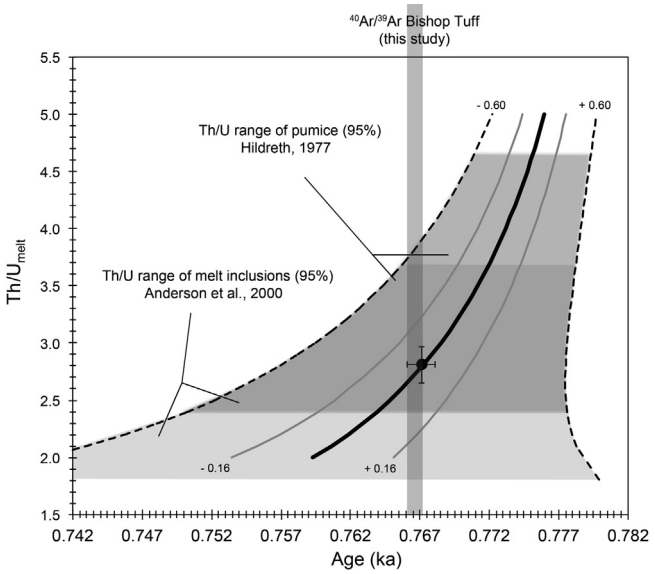

Fig. 10. Plot showing how the estimated Th/U_{melt} composition affects the ID-TIMS U-Pb zircon 'eruption' age (black circle) of Crowley et al. (2007) (*n*17/19). The Th/U_{melt} is treated as a systematic variable, and so this uncertainty is propagated following determination of the weighted mean age. Uncertainty envelopes are shown for the Th/U_{melt} range (±0.16) used by Crowley et al. and what we consider to be a 'more credible' Th/U_{melt} range (±0.60) that reflects *c.* 68% of the variability seen in BT pumice and/or melt inclusions. Of note is the fact that the $^{40}Ar/^{39}Ar$ Bishop Tuff age reported in this study is consistent with the ID-TIMS U-Pb zircon age regardless of what Th/U_{melt} composition is assumed. Note all ages are shown including full external uncertainties and are displayed at the 2-sigma confidence level.

7.6. The MBB and the Bishop Tuff

To define the most accurate age for the North American MBB relative to the BT we adopted the same approach as Sarna-Wojcicki et al. (2000), but built in extra uncertainty to our calculations (as detailed below). We highlight that due to the nature of the terrestrial sections used by Sarna-Wojcicki et al. (2000) (potential for unknown hiatuses in the stratigraphy) this approach is not going to yield a high-precision age constraint, just a useful comparison with the ODP 758 and Channell et al. (2010) MBB ages.

We have made new $^{40}Ar/^{39}Ar$ age determinations on sanidine from the LCTB (Fig. 8), the tuff that postdates the BT in several North American sections that also contain a record of the MBB position (Fig. 12). Single crystal analyses show a LCTB juvenile age population (*n*28) with a robust $^{40}Ar/^{39}Ar$ age of 627.0 ± 1.5/1.7 ka (R^{LCTB}_{ACs}: 0.52734 ± 0.00126). Note that our age for the LCTB is indistinguishable from the $^{40}Ar/^{39}Ar$ age of Matthews et al. (2015) when both are calculated relative to the same calibration

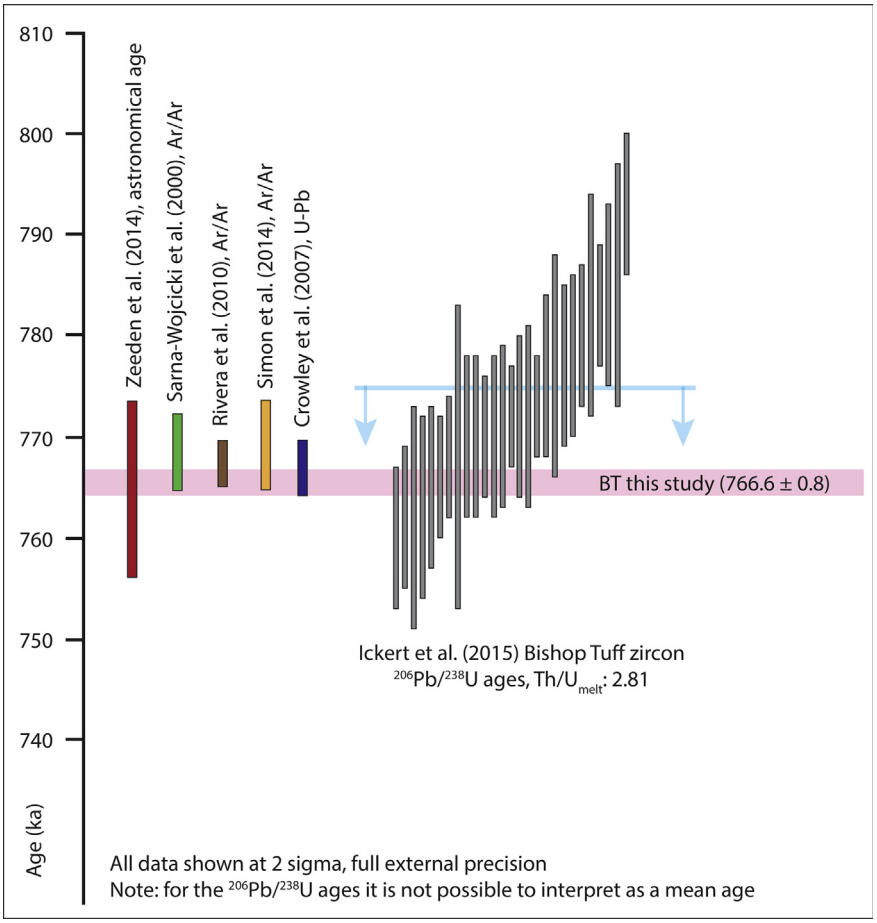

Fig. 11. Geochronological summary plot for the Bishop Tuff. The $^{40}Ar/^{39}Ar$ data of Sarna-Wojcicki et al. (2000), Rivera et al. (2011) and Simon et al. (2014) are shown relative to the BT $^{40}Ar/^{39}Ar$ age presented here. The data are plotted relative to the BT astronomical age of Zeeden et al. (2014) and the ID-TIMS $^{206}Pb/^{238}U$ zircon ages of Ickert et al. (2015). The data are corrected for Th/U_{melt} using a value of 2.81 (Anderson et al., 2000) – the data cannot be interpreted with respect to a mean age as each bulk zircon age is a function of integrating a time-series of crystallisation. Ickert et al. (2015) highlight that with a Th/U_{melt} value of 2.81 the BT probably erupted post-775 ka (blue line in figure). For illustration purposes we have shown the $^{206}Pb/^{238}U$ age reported by Crowley et al. (2007) but see main text for comments concerning use of this 'weighted mean' age. (For interpretation of the references to colour in this figure legend, the reader is referred to the web version of this article.)

(627.4 ± 1.5/1.7 ka, R^{LCTB}_{ACs} 0.52754 ± 0.00124) and is also indistinguishable at the 2 sigma confidence level from the ID-TIMS $^{206}Pb/^{238}U$ LCTB age (629.2 ± 4.3 ka, 2 sigma full uncertainty) reported by Wotzlaw et al. (2015).

As the LCTB postdates the BT we then, following Sarna-Wojcicki et al. (2000), simply calculated the sedimentation rate between LCTB and BT, and subsequently extrapolated Δt from the BT to the MBB in each (n5) individual section (Fig. 13, Table 3). As expected, there is considerable scatter in the extrapolated Δt and MBB ages (MSWD 54) relative to what precision would predict, due most likely to the presence of hiatuses in the stratigraphic sections, either between the LCTB-BT and/or BT-MBB. Therefore, we deem it inappropriate to use the standard error of the mean as a representative uncertainty for the BT-defined MBB age constraint. We choose to use the SEM × SQRT(MSWD) of all five measurements as the most appropriate method for determining a robust uncertainty. Note that we assigned 20% uncertainty to the stratigraphic distances between LCTB, BT and the MBB to also account for potential hiatuses in the stratigraphy at each site (Table 3). The approach defines a MBB age of 789.1 ± 5.6 ka (68.2% confidence). Simply using the average age ± standard deviation of the stratigraphic and age measurements for each sites yields an MBB age of between 776 and 802 ka (Table 3). Both age ranges are resolvable from the proposed MBB age of Channell et al. (2010).

7.7. The age of the MBB

In proposing paradigm-changing shifts in the age of key events within the Geological Time Scale the burden of proof is high. We feel that the data presented here, when considered with respect to the study of Sagnotti et al. (2014), pose serious questions concerning the accuracy of the approaches used previously to date the MBB (for example: Channell et al., 2010). There are now three independent robust and accurate $^{40}Ar/^{39}Ar$ age constraints indicating that current estimations for the age of the MBB are too young. As such, the revision to the Geological Time Scale that we propose has far reaching implications for Quaternary science and other dating techniques.

Taking the two MBB age constraints from this study (ODP 758 and LCTB-BT-MBB) and the MBB age of Sagnotti et al. (2014) we can calculate a weighted average MBB age: 783.4 ± 0.6 ka (R^{MBB}_{ACs} 0.65885 ± 0.00050) (1-sigma, full external precision, MSWD 0.8). We consider this to be currently the most accurate MBB age and the most robust temporal anchor for the Pleistocene Geomagnetic Time Scale. It is *c.* 10.4 ± 1.5 ka older than the MBB age proposed by Channell et al. (2010), and consequently *c.* 3.4 ± 0.7 ka older than the age of the MBB in the LR04 stack (Lisiecki and Raymo, 2005) (or as defined by Shackleton et al., 1990).

We note that our absolute age for the MBB is dependent on

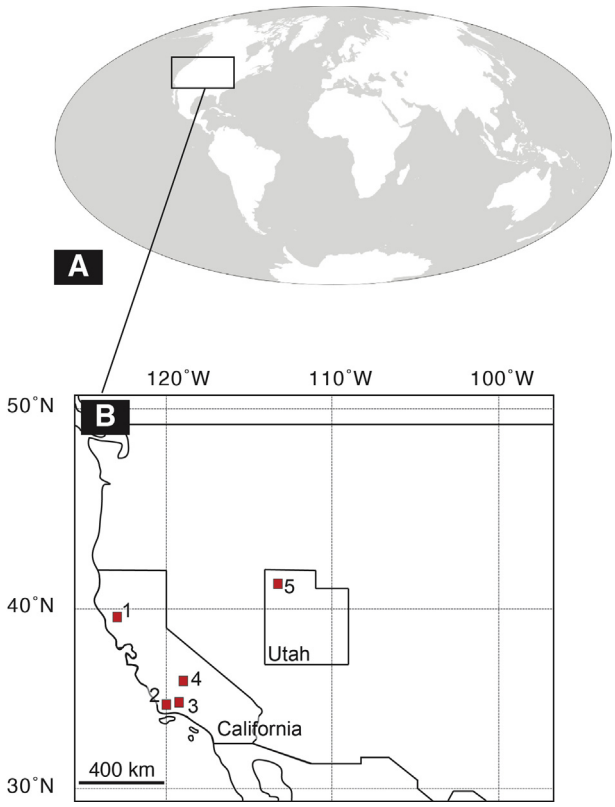

Fig. 12. (A) Map showing region of LCTB-BT-MBB study sites in North America. (B) Location of specific study sites.

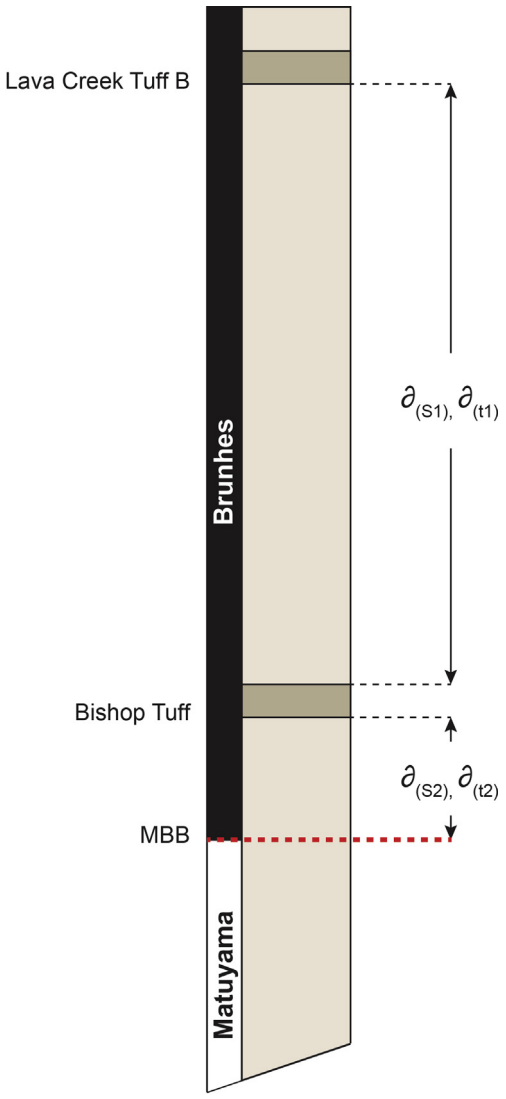

Fig. 13. Schematic drawing showing the relationship between the BT, LCTB and MBB in North America. The symbols correspond to the calculations shown in Table 3.

the specific $^{40}Ar/^{39}Ar$ calibration used, but the difference between employment of the Rivera et al. (2011) calibration and the use of Niespolo et al. (2016) with Renne et al. (2011) results in a MBB age difference of 0.3 ± 2.0 ka. Thus it is inescapable that there are discrepancies between the most precise $^{40}Ar/^{39}Ar$ ages and some (but not all, see discussion below) orbital tuning ages for the MBB.

7.8. Magnetic lock-in delay

It may be questioned whether the ODP 758 MBB age that we present (or the approach we have taken with respect to OPD 758) is biased by delayed acquisition of magnetic remanence (i.e., lock-in) in the sediment (Kent, 1973; Suganuma et al., 2011), owing to a relatively low sedimentation rate. The only possible evidence for this is that the MBB in ODP 758 is not located at the same position within MIS 19 as it is in the high-resolution North Atlantic cores (Channell et al., 2010). There is no doubt that magnetic lock-in delay is a real issue for interpretation of paleomagnetic data from some sediment cores (e.g., Tauxe et al., 1996) but not others (e.g., Valet et al., 2014) and that when assessing such phenomena, we have to consider the level of precision one is achieving when temporally resolving paleomagnetic events relative to any potential lock-in offset.

Typically, the degree of magnetic lock-in delay in marine sediments at the depth of the MBB is minimal (e.g., Tauxe et al., 1996; Bleil and von Dobeneck, 1999; Horng et al., 2002) but in ODP 758 we do not consider lock-in of paleomagnetic remanence as significant, certainly at the depth of the MBB. Our reasoning for this is that there are now three unrelated $^{40}Ar/^{39}Ar$ age constraints for the MBB from three geographically distal sites representing three distinct depositional environments (Sulmona Basin, North America, South China Sea) that are indistinguishable from each other at the 68.2% confidence interval. They yield a weighted mean MBB age with a MSWD of 0.8, revealing no excess scatter in the data as there would be, for example, if paleomagnetic lock-in delay was significant in one of the records. To make an argument for our ODP 758 data being affected significantly by delayed magnetic lock-in would require for the North America MBB record and the Sulmona Basin record to be as equally offset from a younger MBB by exactly the same amount of time. As a consequence, our data now raise two important questions: (1) why is there an offset in the location of the MBB relative to MIS 19 in different records? And (2) why are some orbitally tuned ages for the MBB consistently younger than the most precise and accurate $^{40}Ar/^{39}Ar$ ages?

7.9. Why is there an offset in the location of the MBB relative to MIS 19?

As paleomagnetic lock-in delay in ODP 758 is not significant with respect to the temporal resolution we have achieved, we are left with two possibilities to explain the differences in the ODP 758 MBB location within MIS 19 relative to the high-resolution North

Table 3
MBB extrapolation calculations from North American sections using LCTB-BT and BT-MBB.

LCTB age (ka) BT age (ka)	627.0 ± 1.5 766.6 ± 0.4	Lake Tecopa	Great Salt Lake	Ventura	San joaquin	Fisher valley	
Stratigraphic distance from LCTB to BT	$\partial_{(s1)}$	8.0	9.7	253.0	12.0	21.2	m
Stratigraphic distance from BT to the MBB	$\partial_{(s2)}$	0.5	2.5	18.0	2.5	5.0	m
Time interval from LCTB to BT	$\partial_{(t1)}$	141600	141600	141600	141600	141600	years
Sedimentation rate	$SR = \partial_{(s1)}/\partial_{(t1)}$	0.000056	0.000069	0.001787	0.000085	0.000150	m/year
Time interval BT to MBB	$\partial_{(t2)} = \partial_{(s2)}/SR$	8850	36495	10074	29500	33396	years
MBB age	$BT_{age} + \partial_{(t2)}$	785250	812895	786474	805900	809796	years
MBB age	$BT_{age} + \partial_{(t2)})/1000$	774.5	801.7	775.7	794.8	798.7	ka
± (note 20% uncertainty assigned to all section measurements for extrapolation, ± propagated using linear uncertainty propagation)		1803	1803	1803	1803	1803	years
±		1.8	1.8	1.8	1.8	1.8	ka

Average ± St. Deviation MBB age (relative to the five different sections in N. America) = 776–802 ka.
Mean ± SEM × SQRT(MSWD) MBB age (relative to the five different sections in N. America) = 789.1 ± 5.6 ka (68.2% confidence interval).

Atlantic cores (Channell et al., 2010): (i) it is the position of the MBB that has changed within rock archives across the globe - diachronous onset as suggested by previous modeling of the MB-reversal (Leonhardt and Fabian, 2007; Olson, 2011); or (ii) it is not the position of the MBB that has changed, it is the onset and termination of MIS 19 within marine records that are different across the globe (relative to a fixed position for the geomagnetic reversal).

(i) As Earth's magnetic field intensity drops to low values during polarity reversals the field direction progresses through a 180° change while the field is weak. The time it takes for this process to happen is uncertain. Modeling of the MBB event has suggested reversal durations of between 2 and 10 ka and highlighted potential for a millennial-scale variability in onset of the MB-reversal for sites in the Atlantic and Pacific Oceans (Leonhardt and Fabian, 2007). Such age offsets have not been reported in the literature, although few existing age data are sufficiently precise to resolve diachrony at this scale. A diachronous MBB is supported by the work of Olson (2011) who compared the MBB paleomagnetic trajectories to a complex dynamo model depicting a polarity reversal. Both were initiated by gradual reductions in dipole intensity leading to a reversal precursor event (intensity low) and subsequent transient polarity recovery. Following this was rapid dipole collapse and final directional reversal that began with reverse flux generation in one hemisphere. Virtual geomagnetic poles (VGPs) from sites located proximal to the reverse flux follow complex paths crossing the equator several thousand years prior to the simpler VGP paths from the more distal sites – the magnetic intensity variations produced by the dynamo model reversal correlate with intensity variations inferred for the MBB (Olson, 2011).

These theoretical/model data suggest diachronous onset of the MB-reversal on a time scale that should be resolvable using high-precision radio-isotopic dating. However, our data show temporal coincidence of the MBB at the 68.2% confidence interval for three sites that vary with respect to latitude and longitude. Clement (2004) noted that polarity reversal durations vary with site latitude; low latitude sites have shorter reversal durations than mid-to high-latitude sites. As such, the physical data (analytical measurements) do not appear to support a diachronous MB-reversal model (Leonhardt and Fabian, 2007; Olson, 2011) in which the reversal timing is a systematic function of latitude. Instead, the data support the interpretation that the MB-reversal was a globally isochronous event at the millennial scale.

(ii) Benthic $\partial^{18}O$ (e.g., Fig. 14) is used to align marine records from across the globe. Simplistic tuning of records, or wiggle matching, requires one to make the assumption that the global climate system responds uniformly over millennial time scales. $\partial^{18}O$ change is thought generally to be globally synchronous to within 1 ka – the approximate mixing time of an ocean. This is the fundamental assumption in construction and utillisation of global marine stacks such as LR04 (Lisiecki and Raymo, 2005). Radiocarbon data support this supposition for recent geological time with ^{14}C ages of the Last Glacial Maxima (c. 24 ka) as identified in $\partial^{18}O$ data agree to within 1 ka (Duplessy et al., 1991). If $\partial^{18}O$ changes are not synchronous to within the time it takes the oceans to mix, then any age model that is based on alignment of $\partial^{18}O$ signals would contain significant errors (several ka).

However, the further back in time one goes the greater degrees of offset in $\partial^{18}O$ we can observe, with respect to mixing of the oceans. High-resolution records from the Iberian Margin that chart the last glacial termination (Termination I) provide direct evidence for diachronous benthic $\partial^{18}O$ response with ^{14}C age models showing the Atlantic was leading the Pacific by *c.* 4 ka (Skinner and Shackleton, 2005). The *c.* 4 ka offset would result in an erroneous age model if a stack was constructed or if benthic $\partial^{18}O$ was used as a proxy for ice volume. The mixing of $\partial^{18}O$ throughout the oceans is complicated further by changes in water depth. Studies have demonstrated that it can take an extra 1.5 ka for changes in $\partial^{18}O$ to reach deep-water sites within the same ocean (Labeyrie et al., 2005; Waelbroeck et al., 2006), let alone for $\partial^{18}O$ to be transmitted between shallow and deep water at sites more distal or isolated from the Atlantic.

Lisiecki and Raymo (2009) compared $\partial^{18}O$ records from both sites in the Atlantic and Pacific to assess the respective leads and lags in benthic $\partial^{18}O$. They concluded that $\partial^{18}O$ data show a statistically significant Atlantic lead relative to the Pacific $\partial^{18}O$. For Terminations I-IV a Pacific benthic $\partial^{18}O$ lag of 1.6 ka was estimated and at 128 ka and 330 ka, a *c.* 4 ka lag for the Pacific was determined. It was concluded that such leads-lags, probably generated by diachronous temperature changes (without the requirement for slower circulation), will lead to uncertainties of several ka during glacial terminations and this must be taken in to account when using benthic $\partial^{18}O$ records as a proxy for the timing of ice volume change. Lisiecki and Raymo (2009) note that for different terminations the $\partial^{18}O$ lag could vary dramatically due to the differences in ice volume at the glacial maximum and/or the insolation forcing (Parrenin and Paillard, 2003; Parrenin et al., 2007). Given the increase in lag times between the Atlantic and Pacific Oceans from 1.6

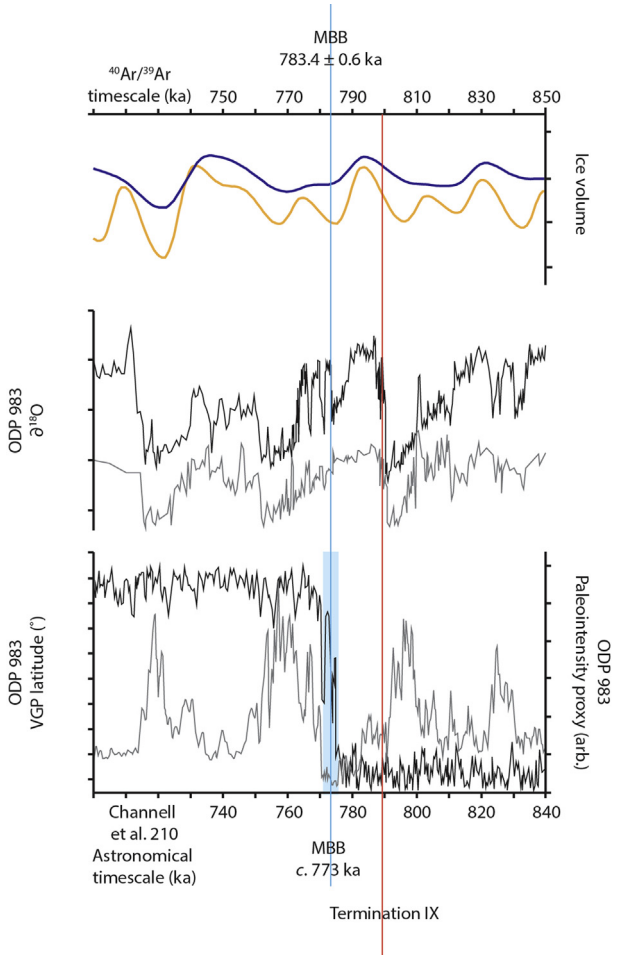

Fig. 14. Plot showing the record for both benthic (grey) and planktic (black) $\partial^{18}O$ from ODP 983 (adapted from Channell et al., 2010). Also shown is Virtual Geomagnetic Polar (VGP) latitude (black) and relative intensity proxy (grey). Ice volume models based on midsummer (orange) and integrated summer (blue) insolation forcing are also plotted. The blue line shows the position of the MBB in the records and the blue box the duration of the MB-reversal at the site of ODP 983 as defined by the benthic $\partial^{18}O$. The lower x-axis shows the astronomical timescale as discussed by Channell et al. (2010 whereas the upper x-axis shows the revised chronology based on the high precision $^{40}Ar/^{39}Ar$ age constraints presented here. (For interpretation of the references to colour in this figure legend, the reader is referred to the web version of this article.)

to 4 ka between Terminations I-IV (20–330 ka) it is currently unclear what the lag time would have been by Termination IX, the termination that pre-dates the MBB (Fig. 14).

These data (Skinner and Shackleton, 2005; Lisiecki and Raymo, 2009) show that the onset and termination of Marine Isotope Stages across the globe cannot, and should not, be considered as synchronous at the level of temporal resolution now attainable using radioisotopic dating. It is also unclear whether we can expect the duration of MIS within different oceans to be the same or whether contraction-expansion of MIS can occur, especially for sites that are proximal or distal to the sites of ice melting (the poles). It is currently impossible to determine accurate age offsets for the MIS times scale between the Atlantic and Pacific, let alone temporally constrain interactions between the Atlantic and other oceans (e.g., Indian Ocean).

Therefore, we contend that within $\partial^{18}O$ records that are obtainable for the Pleistocene there is no requirement for the position of the MBB to be located at the same point in MIS 19. The fact that ODP 758 $\partial^{18}O$ data show the MBB at an earlier position (Fig. 2) in MIS 19 relative to the high-resolution records of the North Atlantic (Channell et al., 2010) should not result in immediate dismissal as evidence of a paleomagnetic 'lock in' delay (Roberts and Winklhofer, 2004; Suganuma et al., 2011). Further, such $\partial^{18}O$ offsets between marine records should not be used as an assessment of the degrees of paleomagnetic lock-in delay (e.g., Horng et al., 2002).

The EU-funded INTIMATE (INTegrating Ice core, MArine and TErrestrial records) network has recognized previously problems of assuming synchronous global response in climate systems and as such, has devised protocols to avoid making such assumptions, which can introduce unquantifiable uncertainties in age models (http://cost-es0907.geoenvi.org). INTIMATE correlations are based on independent tie-points (temporal anchors), which are coupled and compared through the use of either tephra markers (tephrochronology) (e.g., Smith et al., 2013) or accurate/precise chronologies (e.g., Smith et al., 2011; Staff et al., 2013). This approach has led to construction of robust 'event stratigraphies' that have allowed testing of leads and lags in response to climate forcing (Bjorck et al., 1998; Alloway et al., 2007). For 'absolute' dating of processes and events within the Geological Time Scale the INTIMATE approach is more robust than wiggle matching that, at best, allows for relative assessments of time.

7.10. Integration of the astronomical and $^{40}Ar/^{39}Ar$ MBB age

The new age for the MBB is consistent with the astronomical age reported by Chen et al. (1995) for ODP 758. At first sight there appears to be an offset between the MBB age obtained by us using the $^{40}Ar/^{39}Ar$ dating technique and the LR04 stack MBB age (Lisiecki and Raymo, 2005; consequently the astronomical age of Shackleton et al., 1990). However, we do not consider this to be the case - with application of appropriate uncertainties (±5 ka, Martinson et al., 1987) these ages are indistinguishable. We therefore propose our MBB age could now be used as a high-precision tie point in the model of Lisiecki and Raymo (2005) to line up the occurrence of the MBB in marine records (that do not exhibit significant magnetic lock-in effects).

However, the offset with the proposed MBB age of c. 773 ka is real and we suggest there must be uncertainties (beyond reported precision) or errors in the approach of Channell et al. (2010). A detailed review and assessment of astronomical dating and its inherent uncertainties is beyond the scope of this contribution, but we can make some first order observations and pose questions for consideration.

We have already highlighted that previous work has suggested that any astronomically tuned age for the Pleistocene cannot be defined better than to within ± 5 ka (Martinson et al., 1987; Imbrie and Imbrie, 1980). Astronomical ages are derived by wiggle matching climate proxy cycles in sedimentary sequences to either: (1) astronomic solutions (Laskar et al., 2004) for orbital cycles, or (2) calculated solar insolation for a specific latitude and time of year (Milankovitch, 1930; Hays et al., 1976). For example, Fig. 14 shows the planktonic and benthic $\partial^{18}O$ records for ODP 983 relative to ice volume models based on midsummer and integrated summer insolation forcing. If current levels of uncertainties associated with the astronomical dating approach are robust (Martinson et al., 1987), the revision we are proposing (c. 10 ka) to the astronomical MBB age (773 ± 1 ka) of Channell et al. (2010) (relative to our $^{40}Ar/^{39}Ar$ MBB age, 783.4 ± 0.6 ka) is too large to be accounted for by uncertainties in phasing assumptions. Whilst it is true that there are inherent uncertainties associated with the orbital calculations themselves; the orbital solution being sensitive to both shifts in tidal dissipation, and changes in global ice volume that may potentially alter the Earth's dynamical ellipticity (Laskar et al., 1993), other astronomical tuning studies (e.g., Shackleton et al.,

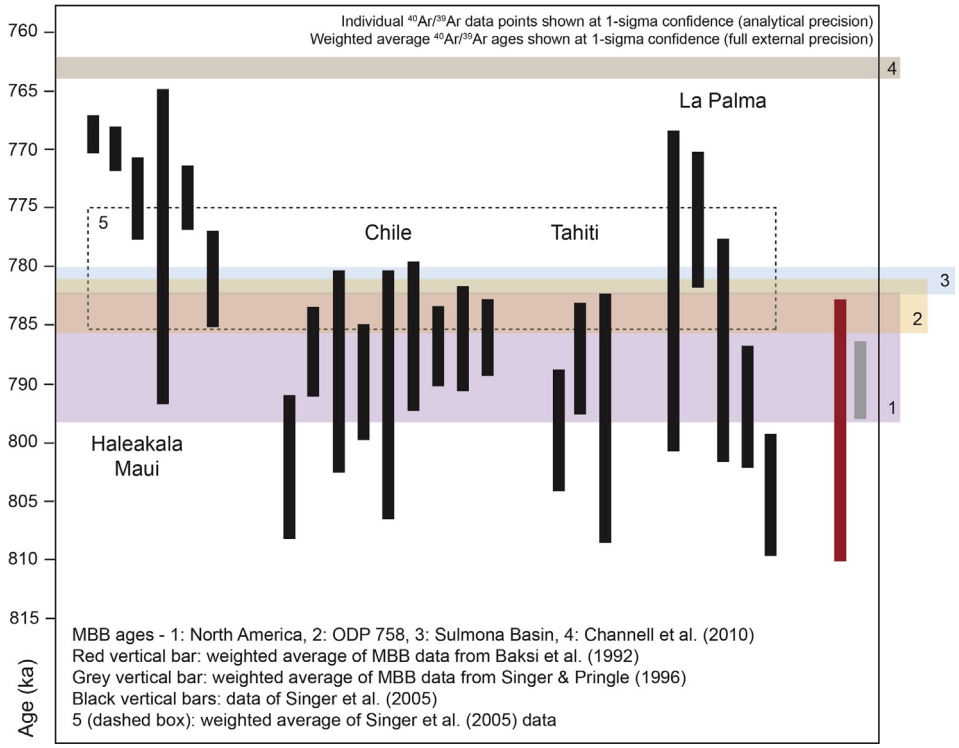

Fig. 15. Plot showing age of transitionally magnetised lava flows (Baksi et al., 1992; Singer and Pringle, 1996; Singer et al., 2005) relative to Renne et al. (2011) and the MBB ages for ODP 758, North America, Sulmona Basin (Sagnotti et al., 2014) and the estimated MBB age of Channell et al. (2010).

1990; Chen et al., 1995) that report MBB ages indistinguishable from our MBB age, use the same orbital calculations which must have the same intrinsic uncertainties/inaccuracies. The remaining possibilities are: (1) orbital sediment cycles may have been mismapped onto orbital forcing by Channell et al. (2010), or (2) the level of precision attained by Channell et al. (2010) is grossly underestimated. It should be noted that although Channell et al. (2010) proposed an error of just ± 1 ka for their MBB age, this represents the standard deviation of the midpoint of the MB-polarity transition for multiple marine records, and not a realistic uncertainty associated with the astronomical dating approach to deriving the MBB age in the Atlantic marine cores.

7.11. The MBB and transitionally magnetized lava flows

As discussed above, $^{40}Ar/^{39}Ar$ ages for transitionally magnetised lava flows have been cited (Baksi et al., 1992; Singer and Pringle, 1996; Coe et al., 2004; Singer et al., 2005; Singer, 2014) as supporting evidence for the astronomical age of the MBB (Channell et al., 2010) and as evidence for a MBB precursor event. There are relatively large age corrections associated with the analysis of low radiogenic ^{40}Ar basaltic-andesitic groundmass that can significantly impact the accuracy of $^{40}Ar/^{39}Ar$ ages (McDougall and Harrison, 1999; Barfod et al., 2014). In comparison to the levels of precision achieved by Sagnotti et al. (2014) and here by the targeting of K-rich sanidine, the level of accuracy and precision attained for dating of young lavas is typically poor, especially if relying on high background isotope extraction techniques such as furnace step-heating (e.g., Singer et al., 2005).

Fig. 15 shows the MBB lava data (Baksi et al., 1992; Singer and Pringle, 1996; Coe et al., 2004; Singer et al., 2005) relative to the proposed ages for the MBB. Note that none of the data are consistent with a MBB age of *c.* 773 ka (Channell et al., 2010) — this observation is independent of which $^{40}Ar/^{39}Ar$ calibration is utilised. Further, whereas it was previously concluded that the data from Chile, Tahiti and La Palma were dating a MBB precursor event, Fig. 15 shows that these data are consistent with our ages for the MBB and the data of Sagnotti et al. (2014). In actual fact, we suggest that the data of Singer et al. (2005) are not dating two events (a MBB precursor event and the MB-reversal) as invoked previously to explain the excess scatter in the data; the data are only dating the MB-reversal, albeit at relatively low accuracy and precision.

The large degree of scatter in data is probably associated with difficulty in dating basaltic-andesitic lava flows. For example, just by examining the data presented from Tahiti (Singer et al., 2005) atmospheric argon contamination ($^{40}Ar_{ATM}$) was accounting for (typically) more than 70% of the total ^{40}Ar budget and thus any small error in this correction would impact age accuracy (but not necessarily age precision). In comparison to sanidine of similar age that we have dated, crystals typically contained *c.* 10% $^{40}Ar_{ATM}$. Hence the corrections are much smaller and easier to make. Most of the single data points of Singer et al. (2005), with the exception of some of the Maui data, are indistinguishable at 95% confidence from the MBB ages at 783.4 ± 0.6 ka when normalized to the same calibration (Fig. 15). Although it is possible that the Maui data are dating a prolonged reversal event (Fig. 15) the work of Sagnotti et al. (2014) suggests the MB-reversal was not of this duration and we consider this scenario unlikely given the reproducible MBB ages we have collected for sites of different latitudes and longitudes - we suggest the data are most likely problematic (inaccurate), certainly at the levels of accuracy and precision that have been reported previously (Singer et al., 2005). Taking this in to consideration we have calculated a weighted average for all the ages for the MBB related lavas (including data from Maui) presented by Singer et al. (2005). We have determined the uncertainty using SEM × SQRT(MSWD) as there is significant scatter in the data

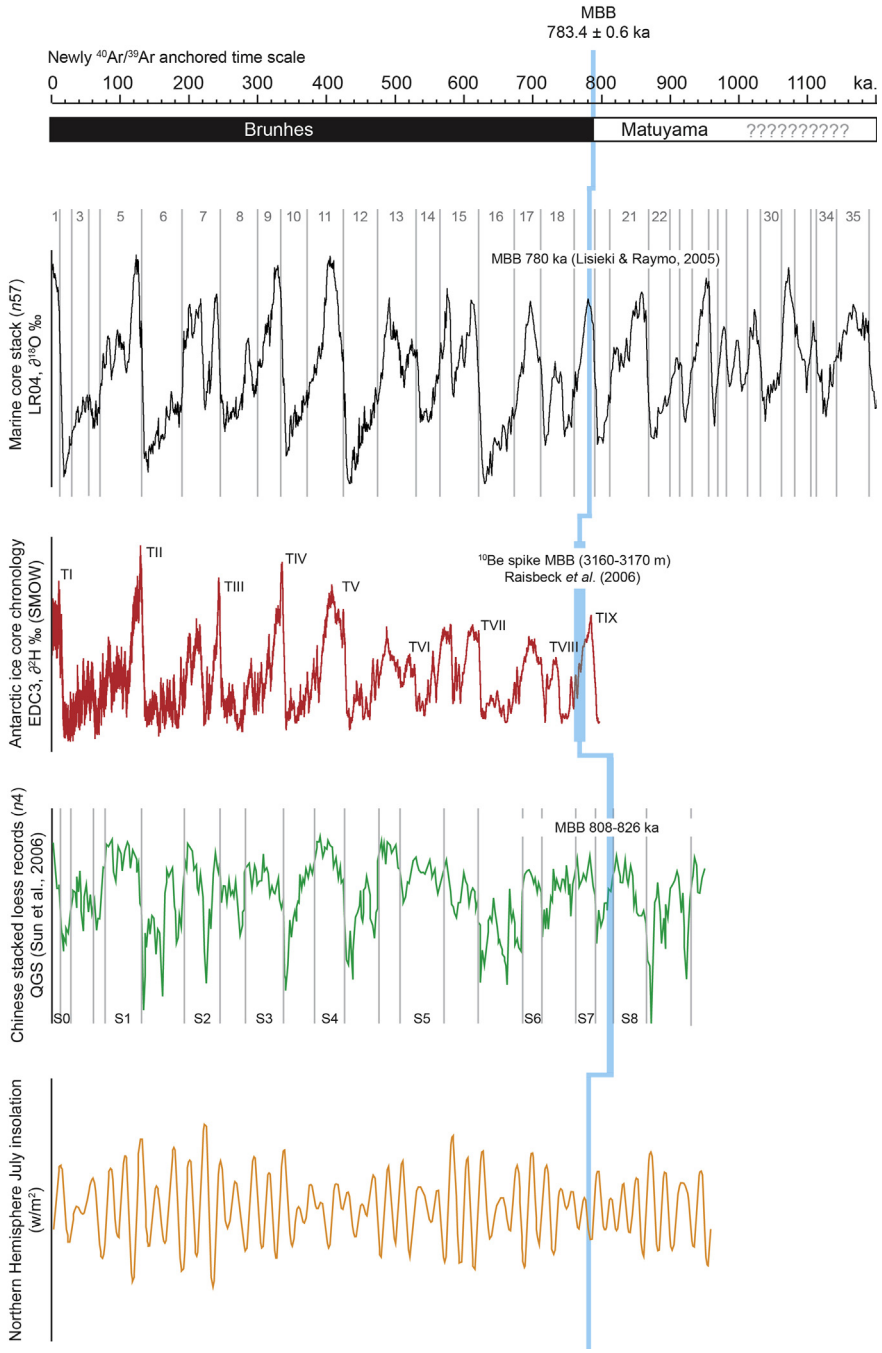

Fig. 16. Plot showing the MBB tie points in multiple records (LR04, Antarctic Ice Core, Chinese Loess Stack) relative to Northern Hemisphere July insolation. Given the lack of evidence for diachronous onset the MBB should be the same age in all records. The upper x-axis shows the newly $^{40}Ar/^{39}Ar$ anchored time scale. Marine Isotope Stages, Glacial Terminations and Chinese loess paleoclimate and paleomagnetic records are all displayed.

(MSWD 7). The resultant age of 779 ± 7.5 ka (1 sigma, full external precision) is indistinguishable from the MBB age we present (783.4 ± 0.6 ka) as well as the astronomically tuned MBB age of 780 ± 5 ka (Lisiecki and Raymo, 2005).

It is important to note that we have not stated that there was not a MBB precursor event, as indeed different records highlight a geomagnetic intensity low prior to the MBB (Kent and Schneider, 1995; Hartl and Tauxe, 1996; Channell et al., 2009, 2010). We are simply stating that the $^{40}Ar/^{39}Ar$ data of Singer et al. (2005) are most likely associated with and dating the MBB. Apart from the age discrepancy reported by Singer et al. (2005) and the explanation invoked to explain this discrepancy, there is no paleomagnetic evidence that the lavas from these sites are related to a MB-reversal precursor event. In fact, the sites were specifically targeted in the first place as they were thought to contain detailed records of the MBB.

7.12. Implications for quaternary age models

Decoupling the age of the MBB from the astronomical time scale and assumptions concerning alignment of $\partial^{18}O$ isotope records allows for independent testing of different Quaternary age models. It is important to realise that our results do not relocate the MBB within the different paleoclimate records; they simply question the

robustness/accuracy of the time scales associated with the paleoclimate records.

Termination IX within ODP 758 is coincident with OTTB at 785.6 ± 0.7/0.8 ka (Fig. 2). Valet et al. (2014) using an astrochronological model determined a Termination IX age of 788–789 (±5) ka from high-resolution Be records across the equatorial Indian Ocean, which allowing for the uncertainties associated with the astronomical tuning approach, is indistinguishable from the ODP 758 age. Further, as Valet et al. (2014) conducted both Be and paleointensity measurements on the same samples we can compare the age of the MBB in ODP 758 with the onset of the MBB from their study. Based on the astronomical age model presented by Valet et al. (2014) the relative paleointensity drop and recovery associated with the MBB occurred at 784 (±5) ka while the cosmogenic Be data indicates reversal onset at 780 (±5) ka - both these ages for the MBB are indistinguishable from our reported MBB age of 783.4 ± 0.6 ka. These data are also commensurate with the age for Termination IX in the LR04 stack (788–789 (±5) ka, Lisiecki and Raymo, 2005).

In addition to now having three independent radioisotopic age constraints (ODP 758, North America sections, Sagnotti et al., 2014) placing the MBB at 783 ± 0.6 ka, the MBB age reported by us is indistinguishable with the astronomical MBB age reported by Shackleton et al. (1990), Chen et al. (1995) Lisiecki and Raymo (2005) and Valet et al. (2014). The implication is that the MB reversal was, at the current levels of temporal resolution, isochronous. There is also agreement between all these records for the age of Termination IX. Our Termination IX age (785.6 ± 0.7/0.8) is also indistinguishable from the age for Termination IX as determined from the Sulmona Basin record (c. 787 ± 2/2 ka) (Giaccio et al., 2015).

Fig. 14 (lower x-axes) shows that the offset between the onset of the MB reversal in the Atlantic Ocean record ODP 983 (Channell et al., 2010) and Termination IX is *c*. 15 ka (Channell et al., 2010). Accepting that the MBB age of Channell et al. (2010) is inaccurate and that the age presented here is correct, as well as assuming that the location of the MBB in the Atlantic records is accurate, then relative to a MBB age of c. 783 ka Termination IX in the Atlantic Ocean should be positioned at c. 798 ka. Does this observation suggest that with respect to the onset of Termination IX, the Atlantic Ocean was leading the Indian Ocean (and terrestrial records) in $\partial^{18}O$ response by *c*. 12 ka?

As discussed previously, Lisiecki and Raymo (2009) did note that for different terminations the $\partial^{18}O$ lag does vary dramatically due to the differences in ice volume at the glacial maximum and/or insolation forcing (Parrenin and Paillard, 2003) with differences of ± 4 ka by Termination IV at 330 ka. If so, then this study and such a large lead-lag between the Atlantic and Indian Oceans further highlights that the dangers of 'wiggle matching' approaches to comparing climate records from across the globe.

We can also use the position of the 'isochronous' MB reversal within multiple paleoclimate archives to correlate between records. Raisbeck et al. (2007) concluded that the enhanced ^{10}Be flux in the EPICA Dome C ice core is a product of low dipole intensity during the MB-transition. Fig. 16 shows the MBB tie point in different records at *c*. 783 ka allowing for correlation between the LR04 stack and EPICA Dome C, as well as correlation to Northern Hemisphere July insolation. The horizontal displacement (along the x-axes) of these tie points shows the inaccuracies in the different time scales currently in use. Our interpretation does not impact the relative temporal offset within a single record, but does highlight that without high-precision independently dated tie points, it is currently not possible to directly compare climatic records from different sources throughout the Pleistocene.

The MBB has also been identified within Chinese loess and red clay sections (Zhou et al., 2014; Wang et al., 2014) but the apparent timing and duration of the MBB remain controversial due to inconsistencies in stratigraphic location. This Chinese record however is of key importance, as it would allow for cryospheric-marine-land correlation of climate records and paleoclimatic reconstruction across reservoirs. If as suggested (Zhou et al., 2014), S7 and S8 within the Chinese loess sections (Fig. 16) correspond to MIS 19 and 21, respectively, then the MBB in the loess significantly pre-dates the MBB elsewhere. Complex post-depositional processes have been invoked to explain the massive downward shift of the MBB in the loess (Suganuma et al., 2010, 2011) but there is another possibility to consider. Several studies have previously proposed that S8 correlates to MIS 19 (Liu et al., 2008; Yang et al., 2010; Wang et al., 2006; Jin and Liu, 2011) and not MIS 21, which then places the MBB in the Chinese loess sections close to the location of the MBB in both the marine records and ice cores. Although this interpretation causes issues for stratigraphic correlation between the loess sections in China (Zhou et al., 2014), we consider it to be the most plausible with respect to the evidence at hand. Fig. 16 shows the proposed correlation and the linkage of S8 to MIS 19.

7.13. ODP 758 defined Australasian Tektite age

The modelled mean age for the Australasian tektite layer (main concentration interval in ODP 758) is 786 ± 2 ka (Fig. 9). The stratigraphic position pre-dates Termination IX, which is positioned at 785.6 ± 0.7/0.8 ka and we consider this modelled age to currently be the most accurate age for the tektites. As the Australasian tektites are found in Indochina, southern China, the Philippines, Malaysia, Indonesia and Australia an accurate age could be used as an isochronous marker horizon across continents (Smith et al., 2011, 2013). In the absence of a crater location, it has been suggested that the impact event that produced the tektites is located in Indochina, probably in close proximity to ODP Hole 1144A (Glass and Koeberl, 2006), but this remains supposition.

8. Conclusions

The present study has (1) provided a robust chronology for the multiple eruptions of the Toba super-volcano, (2) identified a multiple Toba eruption scenario at approximately 800 ka, (3) provided a robust and accurate age for the Australasian tektites, (4) defined robust high-precision ages for the BT and LCTB, (5) allowed for determination of an accurate and precise MBB age of 783.4 ± 0.6 ka, (6) shown at the level of temporal resolution attainable using radioisotopic dating the MB reversal can be considered isochronous, and (6) dated Termination IX in the Indian Ocean. We highlight issues that pose significant challenges to the accuracy of U/Pb zircon dating in the Quaternary and suggest that relative uncertainties at the permil level are unduly optimistic. Finally, at the level of resolution now attainable for Pleistocene climate archives using radioisotopic dating, it is not valid to assume that response to changing $\partial^{18}O$ can be considered synchronous.

As ODP 758 features in the LR04 marine stack, the high-precision $^{40}Ar/^{39}Ar$ ages for the YTT, MTT, OTTA and OTTB, as well as the age for the MBB and Australasian tektites, can be used as temporally accurate and precise anchors. These anchors allow for global-correlation of the geological record, synchronisation of $\partial^{18}O$ climate archives (e.g., ice cores, lake records and speleothems) (e.g., Mark et al., 2014), and for testing of the inter-hemispheric phasing of climate (Shulmeister et al., 2006; Broecker, 1998; Stocker and Johnsen, 2003; Mark et al., 2014). If the misalignment of the

Chinese loess sequences is, as suspected, responsible for placing the MBB relative to MIS 19 in the wrong place, then the MBB tie point can, for the first time, allow for climatic reconstruction and correlation within different paleoclimate archives.

Acknowledgements

DFM thanks NERC for continued funding of the Argon Isotope Facility at SUERC and NERC Faciltiies grant IP/1626/0516. PRR thanks the Ann and Gordon Getty Foundation and the U.S. National Science Foundation (grant BCS-0715465) for support of his work. LM was funded by the Marie Curie FP7 Intra-European Fellowship Program for the duration of this project. VCS acknowledges support from the John Fell Fund, University of Oxford. Sampling at Toba was supported by research grants to Ros F. Muhammad, Department of Geology, University of Malaya, from the Malaysian Ministry of Higher Education (FP079-2007) and Malaysian Ministry of Science, Technology and Innovation (04-01-03-SF0301). Brad Singer, Matt Heizler, Mike Storey and Tiffany Rivera are thanked for discussion concerning the age of the Bishop Tuff and the MBB. Jim Channell is thanked for discussion of MBB timing as recorded in the marine realm. Jim Imlach is thanked for technical assistance. Two reviewers are thanked for detailed comments that have led to significant improvement of this manuscript.

Appendix A. Supplementary data

Supplementary data related to this article can be found at http://dx.doi.org/10.1016/j.quageo.2017.01.002.

References

Alloway, B.V., Lowe, D.J., Barrell, D.J.A., Newnham, R.M., Almond, P.C., Augustinus, P.C., Bertler, N.A.N., Carter, L., Litchfield, N.J., McGlone, M.S., Schulmeister, J., Vandergoes, M.J., Williams, P.W., NZ-INTIMATE members, 2007. Towards a climate event stratigraphy for New Zealand over the past 30 000 years (NZ-INTIMATE project). J. Quat. Sci. 22 (1), 9–35.

Anderson, A.T., Davis, A.M., Lu, F.Q., 2000. Evolution of Bishop Tuff rhyolitic magma based on melt and magnetite inclusions and zoned phenocrysts. J. Petrol. 41 (3), 449–473.

Baksi, A.K., Hsu, V., McWilliams, M.O., Farrar, E., 1992. $^{40}Ar/^{39}Ar$ dating of the Matuyama-Brunhes geomagnetic field reversal. Science 256 (5055), 356–357.

Barfod, D.N., Mark, D.F., Tait, A., Dymock, R.C., Imlach, J., 2014. Argon extraction from geological samples by CO_2 scanning laser step-heating. Geol. Soc. Lond. Spec. Publ. 378 (1), 79–90.

Berger, A.L., Loutre, M.F., 1988. New Insolation Values for the Climate of the Last 10 Million Years. Sc. Report 1988/13. Institut d'Astronomie et de Géophysique G. Lemaître, Université Catholique de Louvain, Louvain-la-Neuve.

Bjorck, S., Walker, M.J.C., Cwynar, L.C., Johnsen, S., Knudsen, K.-L., Lowe, J.J., Wohlfarth, B., 1998. An event stratigraphy for the last termination in the North Atlantic region based on the Greenland ice-core record: a proposal by the INTIMATE group. J. Quat. Sci. 13 (4), 283–292.

Bleil, U., Dobeneck Von, T., 1999. Geomagnetic events and relative paleointensity records—clues to high-resolution paleomagnetic chronostratigraphies of Late Quaternary marine sediments? Use proxies Paleoceanogr. 635–654.

Broecker, W.S., 1998. Paleocean circulation during the last deglaciation: a bipolar seesaw? Paleoceanography 13 (2), 119–121.

Bronk Ramsey, C., Scott, E.M., van der Plicht, J., 2013. Calibration for archaeological and environmental terrestrial samples in the time range 26–50 ka cal BP. Radiocarbon 55 (4), 2021–2027.

Bronk Ramsey, C., 2008. Deposition models for chronological records. Quat. Sci. Rev. 27 (1–2), 42–60.

Bronk Ramsey, C., 2013. OxCal 4.2. Manual [online] available at: https://c14.arch.ox.ac.uk/oxcal.

Bronk Ramsey, C., Lee, S., 2013. Recent and planned developments of the program OxCal. Radiocarbon 55 (2–3), 720–730.

Carey, S., 1997. Influence of convective sedimentation on the formation of widespread tephra fall layers in the deep sea. Geology 25 (9), 839–842.

Chamberlain, K.J., Wilson, C.J.N., Wooden, J.L., Charlier, B.L.A., Ireland, T.R., 2014. New perspectives on the Bishop Tuff from zircon textures, ages and trace elements. J. Petrol. http://dx.doi.org/10.1093/petrology/egt072.

Channell, J.E.T., Xuan, C., Hodell, D.A., 2009. Stacking paleointensity and oxygen isotope data for the last 1.5 Myr (PISO-1500). Earth Planet. Sci. Lett. 283 (1–4), 14–23.

Channell, J.E.T., Hodell, D.A., Singer, B.S., Xuan, C., 2010. Reconciling astrochronological and $^{40}Ar/^{39}Ar$ ages for the Matuyama-Brunhes boundary and late Matuyama Chron. Geochem. Geophys. Geosystems 11 (12).

Chen, C.H., Lee, M.Y., Lizuka, Y., Dehn, J., Wei, K.Y., Carey, S., 2004. First Toba supereruption revival: comment and reply REPLY. Geology 32 (1), 54–55.

Chen, J., Farrell, J.W., Murray, D.W., Warren, L.P., 1995. Timescale and paleoceanographic implications of a 3.6 my oxygen isotope record from the northeast Indian Ocean (Ocean Drilling Program site 758). Paleoceanography 10 (1), 21–47.

Chesner, C.A., Rose, W.I., 1991. Stratigraphy of the Toba tuffs and the evolution of the Toba caldera complex, Sumatra, Indonesia. Bull. Volcanol. 53, 343–356.

Chesner, C.A., Rose, W.I., Deino, A., Drake, R., Westgate, J.A., 1991. Eruptive history of Earth's largest Quaternary caldera (Toba, Indonesia) clarified. Geology 19 (3), 200–203.

Christiansen, R.L., 2001. The Quaternary and Pliocene Yellowstone Plateau Volcanic Field of Wyoming, Idaho, and Montana. US Geological Survey Professional Paper, pp. G1–G145 (729 G).

Clement, B.M., 2004. Dependence of the duration of geomagnetic polarity reversals on site latitude. Nature 428 (6983), 637–640.

Coe, R.S., Singer, B.S., Pringle, M.S., Zhao, X., 2004. Matuyama–Brunhes reversal and Kamikatsura event on Maui: paleomagnetic directions, $^{40}Ar/^{39}Ar$ ages and implications. Earth Planet. Sci. Lett. 222 (2), 667–684.

Crowley, J.L., Schoene, B., Bowring, S.A., 2007. U-Pb dating of zircon in the Bishop Tuff at the millennial scale. Geology 35 (12), 1123–1126.

Dehn, J., Farrell, J.W., Schmincke, H.U., 1991. Neogene tephrochronology from site 758 on northern Ninetyeast Ridge: indonesian arc volcanism of the past 5 Ma. Proc. Ocean Drill. Program, Sci. results 121, 273–295.

Diehl, J., 1987. No short reversals of Brunhes age recorded in the Toba tuffs, North Sumatra, Indonesia. Geophys. Res. Lett. 14 (7), 753–756.

Duplessy, J.C., Bard, E., Arnold, M., Shackleton, N.J., Duprat, J., Labeyrie, L., 1991. How fast did the ocean - atmosphere system run during the last deglaciation? Earth Planet. Sci. Lett. 103 (1–4), 27–40.

Farrell, J.W., Janecek, T.R., 1991. Late neogene paleoceanography and paleoclimatology of the northeast Indian Ocean (site 758). In: Proceedings, Ocean Drilling Program, Scientific Results. 121. Ocean Drilling Program, College Station, Texas, pp. 297–355.

Gee, J., Tauxe, L., Barg, E., 1991. *17*. Lower Jaramillo polarity transition records from the equatorial Atlantic and Indian oceans. In: Proceedings, Ocean Drilling Program, Scientific Results, vol. 121, pp. 377–391.

Giaccio, B., Regattieri, E., Zanchetta, G., Nomade, S., Renne, P.R., Sprain, C.J., Drysdale, R.N., Tzedakis, P.C., Messina, P., Scardia, G., Sposato, A., Bassinot, F., 2015. Duration and dynamics of the best orbital analogue to the present interglacial. Geology 43, 603–606.

Glass, B.P., Koeberl, C., 2006. Australasian microtektites and associated impact ejecta in the South China sea and the middle Pleistocene supereruption of Toba. Meteorit. Planet. Sci. 41, 305–326.

Hall, C.M., Farrell, J.W., 1995. Laser 40Ar/39Ar ages of tephra from Indian Ocean deep-sea sediments: tie points for the astronomical and geomagnetic polarity time scales. Earth Planet. Sci. Lett. 133, 93–94, 327-328.

Hartl, P., Tauxe, L., 1996. A precursor to the Matuyama/Brunhes transition-field instability as recorded in pelagic sediments. Earth Planet. Sci. Lett. 138 (1–4), 121–135.

Hays, J.D., Imbrie, J., Shackleton, N.J., 1976. Variations in the Earth's orbit: pacemaker of the ice ages. Science 194 (4270), 1121–1132.

Horng, C.S., Lee, M.Y., Pälike, H., Wei, K.Y., Liang, W.T., Iizuka, Y., Torii, M., 2002. Astronomically calibrated ages for geomagnetic reversals within the Matuyama chron. Earth Planets Space 54, 679–690.

Hyodo, M., Matsu'ura, S., Kamishima, Y., Kondo, M., Takeshita, Y., Kitaba, I., Danhara, T., Aziz, F., Kurniawan, I., Kumai, H., 2011. High-resolution record of the Matuyama-Brunhes transition constrains the age of Javanese Homo erectus in the Sangiran dome, Indonesia. Proc. Natl. Acad. Sci. U. S. A. 108 (49), 19563–19568.

Ickert, R.B., Mundil, R., Magee Jr., C.W., Mulcahy, S.R., 2015. The U–Th–Pb systematics of zircon from the Bishop Tuff: a case study in challenges to high-precision Pb/U geochronology at the millennial scale. Geochem. Cosmochim. Acta 168, 88–110.

Imbrie, J., Imbrie, J.Z., 1980. Modeling the climatic response to orbital variations. Science 207 (4434), 943–953.

Imbrie, J., Hays, J.D., Martinson, D.G., McIntyre, A., Mix, A.C., Morley, J.J., Pisias, N.G., Prell, W.L., Shackleton, N.J., 1984. The orbital theory of Pleistocene climate: support from a revised chronology of the marine δ18O record. In: Berger, A., Imbrie, J., Hays, H., Kukla, G., Saltzman, B. (Eds.), Milankovitch and Climate: Understanding the Response to Astronomical Forcing, Proceedings of the NATO Advanced Research Workshop Held 30 November - 4 December, 1982 in Palisades, N.Y, p. 269.

Jarosewich, E., Nelen, J.A., Norberg, J.A., 1980. Reference samples for electron microprobe analysis*. Geostand. Newsl. 4 (1), 43–47.

Jin, C., Liu, Q., 2011. Remagnetization mechanism and a new age model for L9 in Chinese loess. Phys. Earth Planet. Interiors 187 (3–4), 261–275.

Jochum, K.P., Stoll, B., Herwig, K., et al., 2006. MPI-DING reference glasses for in situ microanalysis: new reference values for element concentrations and isotope ratios. Geochem. Geophys. Geosystems 7 (2).

Johnson, R.G., 1982. Brunhes-Matuyama magnetic reversal dated at 790,000 yr BP by marine-astronomical correlations. Quat. Res. 17 (2), 135–147.

Katsuta, N., Takano, M., Kawakami, S.I., Togami, S., Fukusawa, H., Kumazawa, M., Yasuda, Y., 2007. Advanced micro-XRF method to separate sedimentary

rhythms and event layers in sediments: its application to lacustrine sediment from Lake Suigetsu, Japan. J. Paleolimnol. 37 (2), 259–271.
Kent, D.V., 1973. Paleomagnetism of some neogene sedimentary rocks on Oga Peninsula, Japan. J. Geomagnetism Geoelectr. 25, 87–103.
Kent, D.V., Schneider, D.A., 1995. Correlation of paleointensity variation records in the Brunhes/Matuyama polarity transition interval. Earth Planet. Sci. Lett. 129 (1–4), 135–144.
Kissel, C., Guillo, H., Laj, C., Carracedo, J.C., Perez-Torrado, F., Wandres, C., et al., 2014. A combined paleomagnetic/dating investigation of the upper Jaramillo transition from a volcanic section at Tenerife (Canary Islands). Earth Planet. Sci. Lett. 406, 59–71.
Knight, M.D., Walker, G., Ellwood, B.B., Diehl, J.F., 1986. Stratigraphy, paleomagnetism, and magnetic fabric of the Toba Tuffs: constraints on the sources and eruptive styles. J. Geophys. Res. 91, 355–382.
Kuiper, K.F., Deino, A., Hilgen, F.J., Krijgsman, W., Renne, P.R., Wijbrans, J.R., 2008. Synchronizing rock clocks of Earth history. Science 320 (5875), 500–504.
Labeyrie, L., Waelbroeck, C., Cortijo, E., Michel, E., Duplessy, J.C., 2005. Changes in deep water hydrology during the Last Deglaciation. Comptes Rendus Geosci. 337 (10–11), 919–927.
Langereis, C.G., Dekkers, M.J., de Lange, G.J., Paterne, M., van Santvoort, P.J.M., 1997. Magnetostratigraphy and astronomical calibration of the last 1.1 Myr from an eastern Mediterranean piston core and dating of short events in the Brunhes. Geophys. J. Int. 129 (1), 75–94.
Lanphere, M.A., Baadsgaard, H., 2001. Precise K–Ar, $^{40}Ar/^{39}Ar$, Rb–Sr and U/Pb mineral ages from the 27.5 Ma fish Canyon tuff reference standard. Chem. Geol. 175 (3–4), 653–671.
Laskar, J., Robutel, P., Joutel, F., Gastineau, M., Correia, A.C.M., Levrard, B., 2004. A long-term numerical solution for the insolation quantities of the Earth. Astronomy Astrophysics 428 (1), 261–285.
Laskar, J., Joutel, F., Robutel, P., 1993. Stabilization of the Earth's obliquity by the moon. Nature 361 (6413), 615–617.
Lee, J.Y., Marti, K., Severinghaus, J.P., Kawamura, K., Yoo, H.S., Lee, J.B., Kim, J.S., 2006. A redetermination of the isotopic abundances of atmospheric Ar. Geochim. Cosmochim. Acta 70 (17), 4507–4512.
Lee, M.Y., Chen, C.H., Wei, K.Y., Iizuka, Y., Carey, S., 2004. First Toba supereruption revival. Geology 32 (1), 61–64.
Leonhardt, R., Fabian, K., 2007. Paleomagnetic reconstruction of the global geomagnetic field evolution during the Matuyama/Brunhes transition: iterative Bayesian inversion and independent verification. Earth Planet. Sci. Lett. 253 (1–2), 172–195.
Lisiecki, L.E., Raymo, M.E., 2005. A Pliocene-Pleistocene stack of 57 globally distributed benthic $\delta^{18}O$ records. Paleoceanography 20 (1).
Lisiecki, L.E., Raymo, M.E., 2009. Diachronous benthic $\delta^{18}O$ responses during late Pleistocene terminations. Paleoceanography 24 (3).
Liu, Q., Roberts, A.P., Rohling, E.J., Zhu, R., Sun, Y., 2008. Post-depositional remanent magnetization lock-in and the location of the Matuyama–Brunhes geomagnetic reversal boundary in marine and Chinese loess sequences. Earth Planet. Sci. Lett. 275 (1–2), 102–110.
Macken, A.C., Staff, R.A., Reed, E.H., 2013. Bayesian age-depth modelling of late quaternary deposits from wet and Blanche caves, naracoorte, south Australia: a framework for comparative faunal analyses. Quat. Geochronol. 17, 26–43.
Mark, D.F., Petraglia, M., Smith, V.C., Morgan, L.E., Barfod, D.N., Ellis, B.S., Pearce, N.J., Pal, J.N., Korisettar, R., 2014. A high-precision $^{40}Ar/^{39}Ar$ age for the Young Toba Tuff and dating of ultra-distal tephra: forcing of Quaternary climate and implications for hominin occupation of India. Quat. Geochronol. 21, 90–103.
Mark, D.F., Petraglia, M., Smith, V.C., Morgan, L.E., Barfod, D.N., Ellis, B.S., Pearce, N.J., Pal, J.N., Korisettar, R., 2013. Multiple interpretive errors? Indeed. Reply to: climate effects of the 74ka Toba super-eruption: multiple interpretive errors in 'A high-precision $^{40}Ar/^{39}Ar$ age for the Young Toba Tuff and dating of ultra-distal tephra' by Michael Haslam. Quat. Geochronol. 18, 173–175.
Mark, D.F., Gonzalez, S., Huddart, D., Böhnel, H., 2010. Dating of the Valsequillo volcanic deposits: resolution of an ongoing archaeological controversy in Central Mexico. J. Hum. Evol. 58 (5), 441–445.
Mark, D.F., Stuart, F.M., de Podesta, M., 2011. New high-precision measurements of the isotopic composition of atmospheric argon. Geochim. Cosmochim. Acta 75 (23), 7494–7501.
Martinson, D.G., Pisias, N., Hays, D.J., Imbrie, J., Moore, T.C., Shackleton, N.J., 1987. Age dating and the orbital theory of the ice ages: development of a high-resolution 0 to 300,000-year chronostatigraphy. Quat. Res. 27, 1–30.
Matthews, N.E., Vazquez, J.A., Calvert, A.T., 2015. Age of the Lava Creek supereruption and magma chamber assembly at Yellowstone based on $^{40}Ar/^{39}Ar$ and U-Pb dating of sanidine and zircon crystals. Geochem. Geophys. Geosystems 16 (8), 2508–2528.
McDougall, I., Harrison, T.M., 1999. Geochronology and Thermochronology by the $^{40}Ar/^{39}Ar$ Method. Oxford University Press, New York.
Milankovitch, M., 1930. Mathematische Klimalehre und Astronomische Theorie der Klimaschwankungen. Handbuch der Klimalogie Band 1 Teil A Borntrager Berlin.
Min, K., Mundil, R., Renne, P.R., Ludwig, K.R., 2000. A test for systematic errors in $^{40}Ar/^{39}Ar$ geochronology through comparison with U/Pb analysis of a 1.1-Ga rhyolite. Geochim. Cosmochim. Acta 64 (1), 73–98.
Morgan, L.E., Mark, D.F., Imlach, J., Barfod, D., Dymock, R., 2014. FCs-EK: a new sampling of the Fish Canyon Tuff $^{40}Ar/^{39}Ar$ neutron flux monitor. Geol. Soc. Lond. Spec. Publ. 378 (1), 63–67.
Niespolo, E.M., Rutte, D., Deino, A.L., Renne, P.R., 2016. Intercalibration and Age of the Alder Creek Sanidine 40Ar/39Ar Standard. Quaternary Geochronology.
Nomade, S., Renne, P.R., Vogel, N., Deino, A.L., Sharp, W.D., Becker, T.A., Jaouni, A.R., Mundil, R., 2005. Alder Creek sanidine (ACs-2): a Quaternary $^{40}Ar/^{39}Ar$ dating standard tied to the Cobb Mountain geomagnetic event. Chem. Geol. 218 (3–4), 315–338.
Olson, P., 2011. Laboratory experiments on the dynamics of the core. Phys. Earth Planet. Interiors 187 (1), 1–18.
Parrenin, F., Paillard, D., 2003. Amplitude and phase of glacial cycles from a conceptual model. Earth Planet. Sci. Lett. 214 (1–2), 243–250.
Parrenin, F., Barnola, J.M., Beer, J., et al., 2007. The EDC3 chronology for the EPICA Dome C ice core. Clim. Past 3, 485–497.
Raisbeck, G., Yiou, F., Jouzel, J., Stocker, T.F., 2007. Direct north-south synchronization of abrupt climate change record in ice cores using Beryllium 10. Clim. Past 3, 541–547.
Reid, M.R., Coath, C.D., 2000. In situ U-Pb ages of zircons from the Bishop Tuff: No evidence for long crystal residence times. Geology 28, 443–446.
Renne, P.R., 2014. Some footnotes to the optimization-based calibration of the $^{40}Ar/^{39}Ar$ system. Geol. Soc. Lond. Spec. Publ. 378, 21–31.
Renne, P.R., Norman, E.B., 2001. Determination of the half-life of ^{37}Ar by mass spectrometry. Phys. Rev. C 63 (4), 047302.
Renne, P.R., Swisher, C.C., Deino, A.L., Karner, D.B., Owens, T.L., DePaolo, D.J., 1998. Intercalibration of standards, absolute ages and uncertainties in $^{40}Ar/^{39}Ar$ dating. Chem. Geol. 145 (1–2), 117–152.
Renne, P.R., Mundil, R., Balco, G., Min, K., Ludwig, K.R., 2010. Joint determination of ^{40}K decay constants and $^{40}Ar^*/^{40}K$ for the Fish Canyon sanidine standard, and improved accuracy for $^{40}Ar/^{39}Ar$ geochronology. Geochim. Cosmochim. Acta 74 (18), 5349–5367.
Renne, P.R., Mundil, R., Balco, G., Min, K., Ludwig, K.R., 2011. Response to the comment by W. H. Schwarz et al. on "Joint determination of ^{40}K decay constants and $^{40}Ar^*/^{40}K$ for the Fish Canyon sanidine standard, and improved accuracy for $^{40}Ar/^{39}Ar$ geochronology. Geochim. Cosmochim. Acta 75, 5097–5100.
Renne, P.R., Deino, A.L., Hilgen, F.J., Kuiper, K.F., Mark, D.F., Mitchell III, W.S., Morgan, L.E., Mundil, R., Smit, J., 2013. Time scales of critical events around the cretaceous-Paleogene boundary. Science 339 (6120), 684–687.
Renne, P.R., Cassata, W.S., Morgan, L.E., 2009. The isotopic composition of atmospheric argon and $^{40}Ar/^{39}Ar$ geochronology: time for a change? Quat. Geochronol. 4 (4), 288–298.
Renne, P.R., Sharp, Z.D., Heizler, M.T., 2008. Cl-derived argon isotope production in the CLICIT facility of OSTR reactor and the effects of the Cl-correction in $^{40}Ar/^{39}Ar$ geochronology. Chem. Geol. 255 (3–4), 463–466.
Rivera, T.A., Storey, M., Zeeden, C., Hilgen, F.J., Kuiper, K., 2011. A refined astronomically calibrated $^{40}Ar/^{39}Ar$ age for Fish Canyon sanidine. Earth Planet. Sci. Lett. 311 (3–4), 420–426.
Rivera, T.A., Storey, M., Schmitz, M.D., Crowley, J.L., 2013. Age intercalibration of $^{40}Ar/^{39}Ar$ sanidine and chemically distinct U/Pb zircon populations from the Alder Creek Rhyolite Quaternary geochronology standard. Chem. Geol. 345, 87–98.
Roberts, A.P., Winklhofer, M., 2004. Why are geomagnetic excursions not always recorded in sediments? Constraints from post-depositional remanent magnetization lock-in modelling. Earth Planet. Sci. Lett. 227 (3–4), 345–359.
Ruddiman, W.F., Raymo, M.E., Martinson, D.G., Clement, B.M., Backman, J., 1989. Pleistocene evolution: northern hemisphere ice sheets and North Atlantic Ocean. Paleoceanography 4 (4), 353–412.
Sagnotti, L., Giaccio, B., Liddicoat, J.C., et al., 2016. How fast was the Matuyama–-Brunhes geomagnetic reversal? A new subcentennial record from the Sulmona Basin, central Italy. Geophys. J. Int. 204 (2), 798–812.
Sagnotti, L., Scardia, G., Giaccio, B., et al., 2014. Extremely rapid directional change during Matuyama-Brunhes geomagnetic polarity reversal. Geophys. J. Int. 199 (2), 1110–1124.
Schlolaut, G., Marshall, M.H., Brauer, A., et al., 2012. An automated method for varve interpolation and its application to the Late Glacial chronology from Lake Suigetsu, Japan. Quat. Geochronol. 13, 52–69.
Shackleton, N.J., Berger, A., Peltier, W.R., 1990. An alternative astronomical calibration of the lower Pleistocene timescale based on ODP Site 677. Trans. R. Soc. Edinb. Earth Sci. 81 (04), 251–261.
Shane, P., Westgate, J., Williams, M., Korisettar, R., 1995. New geochemical evidence for the youngest Toba-Tuff in India. Quat. Res. 44 (2), 200–204.
Shane, P., Self, S., Blake, S., Rampino, M.R., 2004. First Toba supereruption revival: comment and reply. Geology 32 (1), 54.
Shipboard Scientific Party, 1989. doi:10.2973/odp.proc.ir.121.112.1989.
Shulmeister, J., Rodbell, D.T., Gagan, M.K., Seltzer, G.O., 2006. Inter-hemispheric linkages in climate change: paleo-perspectives for future climate change. Clim. Past 2 (2), 167–185.
Simon, J.I., Reid, M.R., 2005. The pace of rhyolite differentiation and storage in an "archetypical" silicic magma system, Long Valley, California. Earth Planet. Sci. Lett. 235 (1–2), 123–140.
Simon, J.I., Weis, D., DePaolo, D.J., Renne, P.R., et al., 2014. Assimilation of preexisting Pleistocene intrusions at Long Valley by periodic magma recharge accelerates rhyolite generation: rethinking the remelting model. Contrib. Mineral. Petrol. 167, 955.
Simon, J.I., Renne, P.R., Mundil, R., 2008. Implications of pre-eruptive magmatic histories of zircons for U-Pb geochronology of silicic extrusions. Earth Planet. Sci. Lett. 266 (1–2), 182–194.
Singer, B.S., 2014. A Quaternary geomagnetic instability time scale. Quat. Geochronol. 21, 29–52.
Singer, B.S., Pringle, M.S., 1996. Age and duration of the Matuyama-Brunhes

geomagnetic polarity reversal from $^{40}Ar^{39}Ar$ incremental heating analyses of lavas. Earth Planet. Sci. Lett. 139 (1–2), 47–61.
Singer, B.S., Hoffman, K.A., Coe, R.S., et al., 2005. Structural and temporal requirements for geomagnetic field reversal deduced from lava flows. Nature 434, 633–636.
Skinner, L.C., Shackleton, N.J., 2005. An Atlantic lead over Pacific deep-water change across Termination I: implications for the application of the marine isotope stage stratigraphy. Quat. Sci. Rev. 24 (5–6), 571–580.
Smit, J., van Eijden, A., Troelstra, S.R., 1991. Analysis of the Australasian microtektite event, the Toba lake event, and the cretaceous/Paleogene boundary, Eastern Indian Ocean. Proc. Ocean Drill. Program, Sci. Results 121, 489–503.
Smith, V.C., Staff, R.A., Blockley, S.P.E., Bronk Ramsey, C., Nakagawa, T., Mark, D.F., Takemura, K., Danhara, T., 2013. Identification and correlation of visible tephras in the Lake Suigetsu SG06 sedimentary archive, Japan: chronostratigraphic markers for synchronising of east Asian/west Pacific palaeoclimatic records across the last 150 ka. Quat. Sci. Rev. 67, 121–137.
Smith, V.C., Mark, D.F., Staff, R.A., Blockley, S.P.E., Bronk Ramsey, C., Bryant, C.L., Nakagawa, T., Han, K.K., Weh, A., Takemura, K., Danhara, T., Suigetsu 2006 Project Members, 2011. Toward establishing precise $^{40}Ar/^{39}Ar$ chronologies for Late Pleistocene palaeoclimate archives: an example from the Lake Suigetsu (Japan) sedimentary record. Quat. Sci. Rev. 30 (21–22), 2845–2850.
Staff, R.A., Nakagawa, T., Schlolaut, G., Marshall, M.H., Brauer, A., Lamb, H.F., Bronk Ramsey, C., Bryant, C.L., Brock, F., Kitagawa, H., van der Plicht, J., Payne, R.L., Smith, V.C., Mark, D.F., Macleod, A., Blockley, S.P.E., Schwenninger, J.L., Tarasov, P.E., Haraguchi, T., Gotanda, K., Yonenobu, H., Yokoyama, Y., Suigetsu 2006 Project Members, 2013. The multiple chronological techniques applied to the Lake Suigetsu SG06 sediment core, central Japan. Boreas 42 (2), 259–266.
Steiger, R.H., Jager, E., 1977. Subcommission on geochronology-convention on use of decay constants in geochronology and cosmochronology. Earth Planet. Sci. Lett. 36, 359–362.
Stoenner, R.W., Oa, S., Katcoff, S., 1965. Half-lives of Argon-37 Argon-39 and Argon-42. Science 148 (3675), 1325.
Stocker, T.F., Johnsen, S.J., 2003. A minimum thermodynamic model for the bipolar seesaw. Paleoceanography 18, 1087.
Storey, M., Roberts, R.G., Saidin, M., 2012. Astronomically calibrated Ar-40/Ar-39 age for the Toba supereruption and global synchronization of late Quaternary records. Proc. Natl. Acad. Sci. U. S. A. 109 (46), 18684–18688.
Suganuma, Y., Yokoyama, Y., Yamazaki, T., Kawamura, K., Horng, C.-S., Matsuzaki, H., 2010. ^{10}Be evidence for delayed acquisition of remanent magnetization in marine sediments: implication for a new age for the Matuyama–Brunhes boundary. Earth Planet. Sci. Lett. 296 (3–4), 443–450.
Suganuma, Y., Okada, M., Horie, K., Kaiden, H., Takehara, M., Senda, R., Kimura, J.-I., Kawamura, K., Haneda, Y., Kazaoka, O., Head, M.J., 2015. Age of Matuyama-Brunhes boundary constrained by U-Pb zircon dating of a widespread tephra. Geology 43 (6), 491–494.
Suganuma, Y., Okuno, J., Heslop, D., Roberts, A.P., Yamazaki, T., Yokoyama, Y., 2011. Post-depositional remanent magnetization lock-in for marine sediments deduced from ^{10}Be and paleomagnetic records through the Matuyama–-Brunhes boundary. Earth Planet. Sci. Lett. 311 (1–2), 39–52.
Tauxe, L., Herbert, T., Shackleton, N.J., York, Y.S., 1996. Astronomical calibration of the Matuyama-Brunhes boundary: consequences for magnetic remanence acquisition in marine carbonates and the Asian loess sequences. Earth Planet. Sci. Lett. 140 (1–4), 133–146.
Valet, J.P., Bassinot, F., Bouilloux, A., Bourlès, D., Nomade, S., Guilloux, V., Lopes, F., Thouveny, N., 2014. Geomagnetic, cosmogenic and climatic changes across the last geomagnetic reversal from Equatorial Indian Ocean sediments. Earth Planet. Sci. Lett. 397, 67–79.
Waelbroeck, C., Levi, C., Duplessy, J.C., Labeyrie, L., Michel, E., Cortijo, E., Bassinot, F., Guichard, F., 2006. Distant origin of circulation changes in the Indian Ocean during the last deglaciation. Earth Planet. Sci. Lett. 243 (1–2), 244–251.
Wang, X., Yang, Z., Lovlie, R., Sun, Z., Pei, J., 2006. A magnetostratigraphic reassessment of correlation between Chinese loess and marine oxygen isotope records over the last 1.1Ma. Phys. Earth Planet. Interiors 159 (1–2), 109–117.
Wang, X., Lovlie, R., Chen, Y., Yang, Z., Pei, J., Tang, L., 2014. The Matuyama–Brunhes polarity reversal in four Chinese loess records: high-fidelity recording of geomagnetic field behavior or a less than reliable chronostratigraphic marker? Quat. Sci. Rev. 101, 61–76.
Wilson, C.J.N., Hildreth, W., 1997. The Bishop Tuff: new insights from eruptive stratigraphy. J. Geol. 105, 407–439.
Wojcicki, A.S., Pringle, M.S., Wijbrans, J., 2000. New $^{40}Ar/^{39}Ar$ age of the Bishop Tuff from multiple sites and sediment rate calibration for the Matuyama-Brunhes boundary. J. Geophys. Res. 105, 21431–21443.
Wotzlaw, J.-F., Bindeman, I.N., Stern, R.A., D'Abzac, F.-X., Schaltegger, U., 2015. Rapid heterogeneous assembly of multiple magma reservoirs prior to Yellowstone supereruptions. Sci. Rep. 5, 1–10.
Wotzlaw, J.F., Schaltegger, U., Frick, D.A., Dungan, M.A., Gerdes, A., Gunther, D., 2013. Tracking the evolution of large-volume silicic magma reservoirs from assembly to supereruption. Geology 41 (8), 867–870.
Wood, Frank, van de Meent, Jan Willem, Mansinghka, Vikash, 2014. A new approach to probabilistic programming inference. In: AISTATS, pp. 2–46.
Yamei, H., 2000. Mid-pleistocene acheulean-like stone technology of the Bose Basin, South China. Science 287 (5458), 1622–1626.
Yang, S., Fang, X., Shi, Z., Lehmkuhl, F., Song, S., Han, Y., Han, W., 2010. Timing and provenance of loess in the Sichuan Basin, southwestern China. Palaeogeogr. Palaeoclimatol. Palaeoecol. 292 (1–2), 144–154.
Zeeden, C., Rivera, T.A., Storey, M., 2014. An astronomical age for the Bishop Tuff and concordance with radioisotopic dates. Geophys. Res. Lett. 41 (10), 3478–3484.
Zhou, W., Beck, J.W., Kong, X., An, Z., Qiang, X., Wu, Z., Xian, F., Ao, H., 2014. Timing of the Brunhes-Matuyama magnetic polarity reversal in Chinese loess using 10Be. Geology 42 (6), 467–470.